CASE FILE
COPY

NACA RM L57B19

NACA

RESEARCH MEMORANDUM

AN ANALYSIS OF VERTICAL-TAIL LOADS MEASURED IN FLIGHT ON A SWEPT-WING BOMBER AIRPLANE

By William A. McGowan and T. V. Cooney

Langley Aeronautical Laboratory
Langley Field, Va.

NATIONAL ADVISORY COMMITTEE
FOR AERONAUTICS

WASHINGTON

May 7, 1957
Declassified October 3, 1957

NATIONAL ADVISORY COMMITTEE FOR AERONAUTICS

RESEARCH MEMORANDUM

AN ANALYSIS OF VERTICAL-TAIL LOADS MEASURED IN FLIGHT ON A SWEPT-WING BOMBER AIRPLANE

By William A. McGowan and T. V. Cooney

SUMMARY

Results are presented of an analysis of vertical-tail shear, bending-moment, and torque loads measured on a swept-wing bomber airplane during rudder-step, rudder-pulse, aileron-roll, and steady-sideslip maneuvers. The flight tests were made at altitudes of 15,000, 25,000, and 35,000 feet and Mach numbers from 0.49 to 0.82.

Lift-curve slopes of the vertical tail obtained from the flight data compared favorably with wind-tunnel and theoretically determined values. The compressibility effect on the vertical-tail lift-curve slope was counteracted by the fuselage flexibility relieving effect.

The center of pressure of the component vertical-tail load due to sideslip was located at approximately 18 percent of the mean aerodynamic chord, and the center of pressure of the rudder-deflection load component was located at approximately 50 percent of the mean aerodynamic chord. The spanwise centers of pressure of both load components were located at about 40 percent of the span.

Static directional-stability derivatives of the airplane and contributions of the vertical tail and wing-fuselage combination to the directional stability of the airplane obtained from the flight data were in good agreement with wind-tunnel values. The wing-fuselage combination was unstable in yaw and all the determined stability derivatives remained effectively constant over the Mach number and dynamic-pressure ranges.

INTRODUCTION

Departures from aircraft designs on which flight data exist raise questions as to the adequacy of design procedures and the accuracy of methods for extending wind-tunnel data to the flight design conditions. In order to aid in checking design procedures and wind-tunnel data and

to present flight data on a swept-wing configuration, the National Advisory Committee for Aeronautics has carried out a comprehensive flight-test program on a swept-wing bomber airplane that includes measurements of loads on the component parts.

This paper presents results of an analysis of shear, bending-moment, and torque loads measured on the vertical tail during rudder-step, rudder-pulse, aileron-roll, and steady-sideslip maneuvers. In order to assess effects of Mach number and altitude, the maneuvers were performed at altitudes of 15,000, 25,000, and 35,000 feet and Mach numbers from 0.49 to 0.82.

The lift-curve slope of the vertical tail and rudder lift-effectiveness factor obtained from flight measurements are compared with wind-tunnel results on a full-scale empennage of the test airplane and with lift-curve slopes and rudder lift-effectiveness factors derived theoretically.

Measured bending-moment and torque values of the vertical tail are resolved to coefficient form, and the coefficients are used to obtain the center of pressure of the sideslip and rudder-deflection load components of the vertical tail.

Static yawing-moment derivatives of the vertical tail, wing-fuselage combination, and airplane obtained from the flight data are compared with wind-tunnel results of a small scale model.

SYMBOLS

b_v	vertical-tail span, ft
b_v'	vertical-tail span outboard of strain-gage station, ft
b_w	wing span, ft
c	local chord of vertical tail, ft
$\bar{c}_1$	mean aerodynamic chord of vertical tail, ft
$\bar{c}_2$	mean aerodynamic chord of vertical-tail area outboard of strain-gage station, ft
$\bar{c}$	mean aerodynamic chord of wing, ft
C_L	vertical-tail lift coefficient, L/qS_v'

C_{L_β} rate of change of vertical-tail lift coefficient with sideslip angle (lift-curve slope), per deg

$\left(C_{L_\beta}\right)_{rigid}$ rate of change of vertical-tail lift coefficient with sideslip angle (fuselage flexibility effect on vertical-tail load removed), per deg

C_{L_β}' rate of change of vertical-tail lift coefficient with effective sideslip angle due to roll, per deg

C_{L_δ} rate of change of vertical-tail lift coefficient with rudder angle, (rudder lift-effectiveness factor), per deg

C_M vertical-tail bending-moment coefficient, $\frac{M}{qS_v'b_v'}$

C_{M_β} rate of change of vertical-tail bending-moment coefficient with sideslip angle, per deg

C_{M_δ} rate of change of vertical-tail bending-moment coefficient with rudder angle, per deg

C_T vertical-tail torque coefficient, $T/qS_v'\bar{c}_2$

C_{T_β} rate of change of vertical-tail torque coefficient with sideslip angle, per deg

C_{T_δ} rate of change of vertical-tail torque coefficient with rudder angle, per deg

C_n airplane yawing-moment coefficient, N/qS_wb_w

$\left(C_{n_\beta}\right)_{WFT}$ rate of change of complete-airplane yawing-moment coefficient with sideslip angle, per deg

$\left(C_{n_\beta}\right)_{WF}$ rate of change of airplane yawing-moment coefficient with sideslip angle (wing-fuselage contribution), per deg

$\left(C_{n_\beta}\right)_T$ rate of change of airplane yawing-moment coefficient with sideslip angle (vertical-tail-load contribution), per deg

$\left(C_{n_\delta}\right)_T$ rate of change of airplane yawing-moment coefficient with rudder angle (rudder-deflection vertical-tail-load contribution), per deg

c.p. center of pressure

d	distance from airplane center-of-gravity water line to vertical tail $\bar{c}_1$, ft
I_Z	airplane yawing moment of inertia, lb-sec^2-ft
l	vertical-tail length, airplane center of gravity to rudder hinge line of $\bar{c}_1$, ft
l'	vertical-tail length, airplane center of gravity to quarter chord of $\bar{c}_2$, ft
L	vertical-tail aerodynamic shear load, lb
L_β	rate of change of vertical-tail shear load with sideslip angle, $\frac{\partial L}{\partial \beta}$, lb/deg
L_δ	rate of change of vertical-tail shear load with rudder angle, $\frac{\partial L}{\partial \delta}$, lb/deg
$L_{\dot{\psi}}$	rate of change of vertical-tail shear load with yawing velocity, $\frac{\partial L}{\partial \dot{\psi}}$, lb/radians/sec
M	vertical-tail aerodynamic bending moment, in-lb
N	yawing moment, ft-lb
q	dynamic pressure, lb/sq ft
S_V	vertical-tail area, sq ft
S_V'	vertical-tail area outboard of strain-gage station, sq ft
S_W	wing area, sq ft
$\frac{S_V l}{S_W b_W}$	tail-volume coefficient
T	vertical-tail aerodynamic torque, in-lb
V	true airspeed, ft/sec
α_e	effective angle of attack of vertical tail, deg

β	sideslip angle at airplane center of gravity, deg
β_t	sideslip angle at vertical tail, deg
δ	rudder angle, deg
δ_a	aileron angle, deg
$\dot{\psi}$	yawing velocity about airplane center of gravity, radians/sec
$\dot{\phi}$	rolling velocity about airplane center of gravity, radians/sec
$\ddot{\psi}$	yawing acceleration about airplane center of gravity, radians/sec^2
σ	sidewash angle at vertical tail, deg
n_t	transverse load factor at vertical tail

Loads, sideslip angles, control deflections, angular velocities, and linear accelerations are incremental values obtained from the trim flight values.

APPARATUS AND TESTS

Test Airplane

A swept-wing jet-propelled medium bomber airplane was used for the tests. (See fig. 1.) Overall dimensions of the test airplane are given in the three-view drawings in figure 2, and other dimensions and characteristics are listed in table I. The plan form of the vertical tail is shown in figure 3 and the ordinates and a sketch of the airfoil section are shown in table II.

Several minor external modifications were made on the airplane to accommodate some of the instrumentation. External changes included the addition of a nose boom and an optigraph fairing on top of the fuselage behind the canopy over the wing center section.

The yaw damper, although part of the standard equipment, was not used during the present tests.

Instrumentation

Standard NACA instruments were used to record airspeed, altitude, angular velocities, accelerations, and angle of sideslip. A boom

extending forward of the fuselage nose, equivalent to a distance of approximately 0.8 of the maximum diameter of the fuselage, housed the airspeed, altitude, angle of attack, and angle-of-sideslip sensing devices. The airspeed system was calibrated in flight and the sideslip angle at the airplane center of gravity was obtained by correcting the measured sideslip angle for the effects of fuselage on the airstream at the sensing vane and for yawing velocity of the airplane about the center of gravity. Angular velocities were measured about the approximate airplane center-of-gravity position. Variable-resistance type of control-position transmitters was used to measure rudder and aileron deflections at the midspan locations.

Strain gages located near the root of the vertical tail (fig. 3) measured structural shears, bending moments, and torques. Torques were measured about axis R_2, which was located at the intersection of the vertical-tail spar and strain-gage station R_1. A strain-gage calibration procedure similar to that outlined in reference 1 was used to combine the primary strain-gage bridges and to obtain equations for structural loads in terms of the gage outputs as recorded on 18-channel oscillographs. Measured structural shears, bending moments, and torques were converted to aerodynamic values by addition of transverse-inertia loads, and the resulting aerodynamic loads were used in the analysis.

The bulk of the recording instruments was installed in the bomb-bay section of the fuselage; however, control-position transmitters, airspeed-recording instruments, some accelerometers, and so forth, were located at various points in the fuselage and tail.

A time pulse of one-tenth second correlated the records of all recording instruments.

Estimated Accuracies

The following accuracies of the measured quantities were estimated:

Sideslip angle, β, deg	±0.1
Rudder angle, δ, deg	±0.2
Aileron angles, δ_a, deg	±0.2
Yawing velocity, $\dot{\psi}$, radian/sec	±0.003
Mach number	±0.01
Vertical-tail shear load, L, lb	±100
Vertical-tail bending moment, M, in-lb	±6,000
Vertical-tail torque, T, in-lb	±8,000

Test Maneuvers

The flight-test maneuvers analyzed were a series of rudder-step, rudder-pulse, aileron-roll, and steady-sideslip runs at altitudes of 15,000, 25,000, and 35,000 feet over a Mach number range from 0.49 to 0.82. Variations of Reynolds number with Mach number at the three test altitudes are shown in figure 4. Reynolds numbers are based on the vertical-tail mean aerodynamic chord $\bar{c}_l$. Maneuvers were initiated with the airplane in the clean configuration (that is, landing gear and flaps up) and trimmed for straight and level flight. The center-of-gravity position, airspeed, and altitude remained effectively constant during any particular test run.

Brief descriptions of the four types of maneuvers analyzed are now given. Positive directions of the measured quantities are given on a schematic sketch of the airplane in figure 5. The direction given for positive yawing velocity is the opposite of convention.

The rudder-step maneuver was initiated by an abrupt rudder deflection. This rudder deflection was held constant until after the airplane reached maximum sideslip angle. The rudder-pulse maneuver consisted of an abrupt rudder deflection to a maximum and back to neutral. In aileron-roll maneuvers, the ailerons were abruptly deflected and held constant until the airplane reached approximately 60° of bank at which time the records were turned off and recovery started. Except for the initiating control movement, all other controls were not deflected from trim for these maneuvers.

The steady sideslips were quasi-steady maneuvers. The airplane was stabilized in constant-heading sideslip with required rudder, aileron, and elevator deflections. Maneuvers were performed in groups; each group was at one Mach number and consisted of stabilized runs at different sideslip angles starting at zero sideslip.

Time histories of measured values for typical rudder-step, rudder-pulse, and aileron-roll maneuvers are shown in figures 6, 7, and 8, respectively. Circled points given in these plots represent values at times for which the flight records were read and used directly in the analysis.

METHODS OF ANALYSIS OF FLIGHT DATA

For the derivation of the vertical-tail parameters from the flight data, the aerodynamic load on the vertical tail was defined in terms of the sideslip angle of the vertical tail. For the derivation of airplane

yawing-moment parameters from the data, the vertical-tail load was considered to be the load required to balance the yawing moment of the wing-fuselage combination.

Vertical-Tail Parameters

The incremental shear load L on the vertical tail was defined, in terms of incremental angles of sideslip at the tail, as the sum of the following component loads:

$$L = \left\{ \begin{array}{ll} \left(C_{L_\beta}\right)_{rigid} \beta\left(1 + \frac{d\sigma}{d\beta}\right) qS_v' + & \text{(a)} \\ \left(C_{L_\beta}\right)_{rigid} \frac{\dot{\psi} l'}{V} qS_v' + & \text{(b)} \\ \left(C_{L_{\beta'}}\right)_{rigid} \frac{\dot{\phi} d}{V} qS_v' + & \text{(c)} \\ \left(C_{L_\beta}\right)_{rigid} \frac{d\sigma}{d\beta} \frac{l'}{V} \dot{\beta} qS_v' + & \text{(d)} \\ \left(C_{L_\delta}\right)_{rigid} \delta qS_v' + & \text{(e)} \\ \left(C_{L_\beta}\right)_{rigid} \Delta\beta_t \, qS_v' + & \text{(f)} \\ \left(C_{L_\beta}\right)_{rigid} \eta_t \frac{d\beta}{d\eta} qS_v' & \text{(g)} \end{array} \right\} \text{Component} \qquad (1)$$

where the terms are arranged to identify the component loads associated with:

(a) Sideslip angle measured at airplane center of gravity and the sidewash angle, at the vertical tail

(b) Incremental sideslip angle due to yawing velocity about the airplane center of gravity

(c) Vertical-tail angle of attack due to rolling velocity

(d) Sidewash angle at vertical tail which is due to rate of change of sideslip angle

(e) Rudder deflection

(f) Angle-of-sideslip change at the tail which results from a fuselage deflection due to vertical-tail load

(g) Angle-of-sideslip change at the tail which results from a fuselage deflection due to transverse-inertia fuselage loading

The first five component loads ((a) to (e)) listed in equation (1) have been generally used in the past to define vertical-tail load when a rigid-airplane structure was assumed. However, in order to indicate the effects of fuselage flexibility the last two terms ((f) and (g)) are included. Preliminary analysis of the data revealed that the rolling-velocity and transverse-acceleration components ((c) and (g), respectively) were small and could be dropped. Also it was assumed that the dynamic pressure at the tail was equal to that measured at the nose boom, and the sidewash was considered to be negligible. With these assumptions, equation (1) is simplified to the form

$$L = \left(C_{L_\beta}\right)_{\text{rigid}} qS_v'\left(\beta + \Delta\beta_t\right) + \left(C_{L_\beta}\right)_{\text{rigid}} qS_v' \frac{l'}{V}\dot{\psi} + \left(C_{L_\delta}\right)_{\text{rigid}} qS_v'\delta$$

The coefficient $\left(C_{L_\beta}\right)_{\text{rigid}}$ represents the rate of change of vertical-tail lift coefficient with effective vertical-tail sideslip angle, and $\left(C_{L_\delta}\right)_{\text{rigid}}$ represents the rudder lift-effectiveness factor for the vertical tail.

In order to evaluate the incremental angle of attack $\Delta\beta_t$, use was made of data presented in reference 2 which showed that due to fuselage bending an effective vertical-tail angle of sideslip of 0.42° was developed

for a 10,000-pound vertical-tail load. The vertical-tail load was therefore considered to deflect the fuselage and change the vertical-tail angle by the factor $\Delta\beta_t = \frac{-0.42L}{10000}$. Then substituting for $\Delta\beta_t$ and solving for L in the simplified equation gives:

$$L = \left[\frac{(C_{L_\beta})_{rigid}}{1 + (C_{L_\beta})_{rigid}\, qS_v' \frac{0.42}{10000}}\right] qS_v'\beta +$$

$$\left[\frac{(C_{L_\beta})_{rigid}}{1 + (C_{L_\beta})_{rigid}\, qS_v' \frac{0.42}{10000}}\right] qS_v' \frac{l'}{V} \dot{\psi} +$$

$$\left[\frac{(C_{L_\delta})_{rigid}}{1 + (C_{L_\beta})_{rigid}\, qS_v' \frac{0.42}{10000}}\right] qS_v'\delta \qquad (2)$$

Bracketed terms in equation (2) define the rate of change of vertical-tail lift coefficient with airplane sideslip angle C_{L_β} and the rate of change of vertical-tail lift coefficient with rudder angle C_{L_δ}.

Lift-curve slopes C_{L_β} and C_{L_δ} for the flexible airplane are therefore defined from equation (2) as

$$C_{L_\beta} = \frac{(C_{L_\beta})_{rigid}}{1 + (C_{L_\beta})_{rigid}\, qS_v' \frac{0.42}{10000}} \qquad (3)$$

and

$$C_{L_\delta} = \frac{(C_{L_\delta})_{rigid}}{1 + (C_{L_\beta})_{rigid}\, qS_v' \frac{0.42}{10000}} \qquad (4)$$

For use in the analysis, equations (3) and (4) are then solved as follows:

$$\left(C_{L_\beta}\right)_{\text{rigid}} = \frac{C_{L_\beta}}{1 - C_{L_\beta} q S_v' \frac{0.42}{10000}} \tag{5}$$

and

$$\left(C_{L_\delta}\right)_{\text{rigid}} = \frac{C_{L_\delta}}{1 - C_{L_\beta} q S_v' \frac{0.42}{10000}} \tag{6}$$

and the values of C_{L_β} and C_{L_δ} used were obtained from the flight measurements.

Lift-curve parameters.- The two lift-curve slopes C_{L_β} and C_{L_δ} were derived from the flight data with a modified form of equation (2). The quantities L, β, $\dot{\psi}$, δ, q, S_v', V, and l' in equation (2) were available from flight measurements and the geometric characteristics. The following equation can be obtained by combining the first two product terms in equation (2):

$$L = \left(L_\beta\right)\left(\beta + \frac{l'}{V}\dot{\psi}\right) + \left(L_\delta\right)\delta$$

From experience it is known that a solution of this equation by the least-squares methods gives smaller probable errors if the three constants and variables are arranged on the right-hand side as

$$L = \left(L_\beta\right)\beta + \left(L_{\dot{\psi}}\right)\dot{\psi} + \left(L_\delta\right)\delta \tag{7}$$

As a first step in the derivation of lift-curve slopes C_{L_β} and C_{L_δ} for the flexible airplane from equation (7), the flight records were read at selected times during each dynamic maneuver to give a good representation of record time history for each run. A typical selection of times at which records were read for a rudder-kick maneuver is shown in figure 6. Times at which the records were read for each run established the number of equations to be normalized in solving for C_{L_β} and

C_{L_δ} by a least-squares procedure. (See eq. (7).) In the example given in figure 6, there were 45 simultaneous equations with the 3 unknowns L_β, L_δ, and $L_{\dot{\psi}}$. The parameters C_{L_β} and C_{L_δ} were found for each dynamic maneuver listed in table III. A value of C_{L_β} was obtained from each of the load terms L_β and $L_{\dot{\psi}}$. However, only the C_{L_β} derived from the L_β term is presented because the component load due to sideslip (eq. (7)) was generally much larger than the yawing-velocity component load (eq. (7)).

In steady sideslips, unlike the dynamic maneuvers, the sideslip angle varied linearly with rudder deflection and vertical-tail load. The sideslips did not, therefore, permit a least-squares analysis of the data because the resulting equations would have been redundant. Results from the steady sideslips were used, however, in deriving the yawing-moment parameter of the wing-fuselage combination.

C_M and C_T parameters.- Vertical-tail bending-moment and torque parameters C_{M_β}, C_{M_δ}, C_{T_β}, and C_{T_δ} were also obtained from the flight data with least-squares methods similar to those used in finding the flight lift-curve slopes. The following equations are used in determining the flexible-airplane parameters:

$$M = C_{M_\beta} q S_v' b_v' \beta + C_{M_\beta} q S_v' b_v' \frac{l'}{V} \dot{\psi} + C_{M_\delta} q S_v' b_v' \delta$$

and

$$T = C_{T_\beta} q S_v' \bar{c}_2 \beta + C_{T_\beta} q S_v' \bar{c}_2 \frac{l'}{V} \dot{\psi} + C_{T_\delta} q S_v' \bar{c}_2 \delta$$

which may be simplified and are given as follows:

$$M = \left(M_\beta\right)\beta + \left(M_{\dot{\psi}}\right)\dot{\psi} + \left(M_\delta\right)\delta \tag{8}$$

and

$$T = \left(T_\beta\right)\beta + \left(T_{\dot{\psi}}\right)\dot{\psi} + \left(T_\delta\right)\delta \tag{9}$$

where terms in the parentheses are the unknowns.

The bending-moment and torque parameters for a rigid-fuselage case $\left(C_{M_\beta}\right)_{rigid}$, $\left(C_{M_\delta}\right)_{rigid}$, $\left(C_{T_\beta}\right)_{rigid}$, and $\left(C_{T_\delta}\right)_{rigid}$ were also derived from flight data with equations similar to equations (5) and (6). The specific equations used were

$$\left(C_{M_\beta}\right)_{rigid} = \frac{C_{M_\beta}}{1 - C_{L_\beta}\left(\frac{0.42}{10000}\right)qS_v'} \tag{10}$$

$$\left(C_{M_\delta}\right)_{rigid} = \left(C_{M_\beta}\right)_{rigid}\left(\frac{0.42}{10000}\right)qS_v'C_{L_\delta} + C_{M_\delta} \tag{11}$$

and

$$\left(C_{T_\beta}\right)_{rigid} = \frac{C_{T_\beta}}{1 - C_{L_\beta}\left(\frac{0.42}{10000}\right)qS_v'} \tag{12}$$

$$\left(C_{T_\delta}\right)_{rigid} = \left(C_{T_\beta}\right)_{rigid}\left(\frac{0.42}{10000}\right)qS_v'C_{L_\delta} + C_{T_\delta} \tag{13}$$

Center of pressure.- Spanwise and chordwise center-of-pressure locations for the sideslip and rudder-deflection vertical-tail load components were obtained from flight data. The following relations give the spanwise locations for sideslip and rudder deflections.

$$\frac{M}{L} = \frac{\left(C_{M_\beta}\right)_{rigid}\beta qS_v b_v}{\left(C_{L_\beta}\right)_{rigid}\beta qS_v} = \frac{\left(C_{M_\beta}\right)_{rigid}}{\left(C_{L_\beta}\right)_{rigid}}b_v \tag{14}$$

$$\frac{M}{L} = \frac{\left(C_{M_\delta}\right)_{rigid}\delta qS_v b_v}{\left(C_{L_\delta}\right)_{rigid}\delta qS_v} = \frac{\left(C_{M_\delta}\right)_{rigid}}{\left(C_{L_\delta}\right)_{rigid}}b_v \tag{15}$$

and the chordwise locations for sideslip and rudder deflections are:

$$\frac{T}{L} = \frac{\left(C_{T_\beta}\right)_{rigid}\beta qS_v\bar{c}_l}{\left(C_{L_\beta}\right)_{rigid}\beta qS_v} = \frac{\left(C_{T_\beta}\right)_{rigid}}{\left(C_{L_\beta}\right)_{rigid}}\bar{c}_l \tag{16}$$

$$\frac{T}{L} = \frac{\left(C_{T_\delta}\right)_{\text{rigid}} \delta q S_v \bar{c}_l}{\left(C_{L_\delta}\right)_{\text{rigid}} \delta q S_v} = \frac{\left(C_{T_\delta}\right)_{\text{rigid}}}{\left(C_{L_\delta}\right)_{\text{rigid}}} \bar{c}_l \tag{17}$$

The tail-load parameters C_L, C_M, and C_T required in the equations (14), (15), (16), and (17) were derived previously from equations (7), (8), and (9) and corrected to the rigid-fuselage case with equations (5), (6), (10), (11), (12), and (13).

Airplane Yawing-Moment Parameters

In addition to determining tail parameters, the data for the flexible airplane were analyzed to obtain other quantities.

Airplane moment of inertia.- The yawing moment of inertia of the airplane I_z was determined from flight data by using the expression

$$I_z = \frac{L}{\ddot{\psi}} l \tag{18}$$

Vertical-tail loads and yawing accelerations obtained during the first part of rudder-step maneuvers, when sideslip angle and rolling velocity are effectively zero, were used to determine the yawing moment of inertia of the airplane. A plot was made of maximum vertical-tail loads and maximum rates of change of yawing velocities measured near the start of each maneuver. The slope of this curve, vertical-tail load per radian per second per second, was used in equation (18) to calculate the airplane yawing moment of inertia.

Contribution of vertical tail and rudder.- The airplane yawing moment contributed by the vertical tail was established from flight data as follows:

$$N = \left(C_{n_\beta}\right)_T \beta q S_w b_w = C_{L_\beta} \beta q S_v l$$

so that the following contribution from the tail resulted:

$$\left(C_{n_\beta}\right)_T = C_{L_\beta} \frac{S_v l}{S_w b_w} \tag{19}$$

Values of C_{L_β} determined for the flexible airplane from the least-squares analysis of the flight data (equation (7)) and the tail lengths l listed in table III were used in equation (19) to calculate $\left(C_{n_\beta}\right)_T$.

In a similar manner the airplane yawing-moment contribution of the vertical-tail load due to rudder deflection was defined by

$$\left(C_{n_\delta}\right)_T = C_{L_\delta} \frac{S_V l}{S_w b_w} \tag{20}$$

and the previously determined values of C_{L_δ} for the flexible airplane were used to calculate the tail contribution $\left(C_{n_\delta}\right)_T$.

Contribution of wing-fuselage.- The wing-fuselage contribution to the airplane yawing moment was determined from flight measurements made in steady sideslips. Since in a steady sideslip the vertical-tail load is required to balance the yawing moment of the wing-fuselage combination, the sum of the yawing moments on the quasi-steady airplane must equal zero. Therefore,

$$Ll + N_{WF} = 0$$

or

$$Ll + \left(C_{n_\beta}\right)_{WF} \beta q S_w b_w = 0$$

from which

$$\left(C_{n_\beta}\right)_{WF} = \frac{-Ll}{\beta q S_w b_w} \tag{21}$$

Since quantities on the right side of equation (21) were known, either from the listed geometric characteristics or measured in flight (at one time during each of the steady-sideslip maneuvers), the relation was solved for the wing-fuselage yawing-moment coefficient.

Airplane static directional stability.- The static-yawing-moment coefficient for the complete airplane $\left(C_{n_\beta}\right)_{WFT}$ was derived from the flight data by two methods.

The coefficient $\left(C_{n_\beta}\right)_{WFT}$ was determined from the simplified method given in reference 3 in which

$$\left(C_{n_\beta}\right)_{WFT} = \frac{4\pi^2}{57.3} \frac{I_z}{qS_w b_w P^2} \tag{22}$$

where P, the period of yawing oscillation, was found from flight records of yawing velocity during rudder-pulse maneuvers when all controls were held fixed after the rudder pulse. The value of I_z in this equation was previously found from the flight data.

A second method used to obtain $\left(C_{n_\beta}\right)_{WFT}$ was to add the previously obtained yawing-moment coefficients of the vertical tail and of the wing-fuselage combination. Thus,

$$\left(C_{n_\beta}\right)_{WFT} = \left(C_{n_\beta}\right)_{WF} + \left(C_{n_\beta}\right)_{T} \tag{23}$$

RESULTS AND DISCUSSION

Maximum rates of change of rudder and total-aileron deflections were determined for each maneuver from time-history data such as are given in figures 6, 7, and 8. These rates plotted against dynamic pressure are given in figures 9 and 10 for the rudder and ailerons, respectively. The small insert indicates the manner in which the rates were established. Control rates shown in these figures do not represent the maximum obtainable by the pilot but the maximum used in the particular test.

The main results of the analysis are presented under two general headings: (a) vertical-tail parameters, and (b) airplane yawing-moment parameters. Also presented are theoretical values of vertical-tail parameters as well as the dynamic-overyaw factor and directional control effectiveness of the airplane.

Vertical-Tail Parameters

Variations of tail lift-curve slopes $\left(C_{L_\beta}\right)_{rigid}$ and $\left(C_{L_\delta}\right)_{rigid}$, derived from flight data with equation (7) and corrected for fuselage flexibility by equations (5) and (6) to represent an assumed rigid-airplane case, are shown in figure 11. Also shown in figure 11 are

theoretical values of $(C_{L_\beta})_{rigid}$ and $(C_{L_\delta})_{rigid}$ and low-speed wind-tunnel values corrected for compressibility that were used in design of the vertical tail.

Theoretical vertical-tail lift-curve slopes $(C_{L_\beta})_{rigid}$ and $(C_{L_\delta})_{rigid}$ were established by using the methods and information presented in references 4, 5, 6, and 7 when a rigid fuselage was assumed. In applying these methods, the section lift-curve slope used for the BAC 100 airfoil was 6.19 which is the value given in reference 8 for a similar airfoil. As suggested in references 4 and 6, the geometric aspect ratio of the vertical tail was increased 1.5 times to correct for end-plate effects of the horizontal tail and fuselage. All other quantities used in evaluating the theoretical values of $(C_{L_\beta})_{rigid}$ and $(C_{L_\delta})_{rigid}$ were obtained from the vertical-tail geometric characteristics.

The theoretical $(C_{L_\beta})_{rigid}$ curve is generally within the scatter of flight values, and the design curve envelopes the flight data. Agreement in both instances is considered to be good. The theoretical low-speed value $(M = 0.14)$ of $(C_{L_\beta})_{rigid}$ is 0.046 but is not shown in figure 11, and a design value of 0.054 was obtained from reference 9.

Values of the theoretical $(C_{L_\delta})_{rigid}$ curve were generally more positive than the flight values. Flight values of $(C_{L_\delta})_{rigid}$ did not increase with Mach number as did the theoretical values, possibly because of rudder twist. The low-speed design value of 0.022 for $(C_{L_\delta})_{rigid}$ approximated the flight values throughout the Mach number range.

It is to be noted that $(C_{L_\beta})_{rigid}$ obtained from rudder-pulse data are not plotted in figure 11, although they were determined from the routine solution of equation (7). In the rudder-pulse maneuvers, the sideslip angle reached by the airplane and, hence, the resulting vertical-tail load component due to β were small. Associated values of $(C_{L_\beta})_{rigid}$ were consequently less reliable than those obtained in the step maneuvers. In a similar category were values of $(C_{L_\delta})_{rigid}$ derived from aileron-roll maneuvers where rudder deflection was zero, or nearly so, and the related rudder-deflection load component was small. Values of $(C_{L_\delta})_{rigid}$ determined from aileron rolls were not reliable and are not shown in figure 11.

Variations of parameters C_{L_β} and C_{L_δ} with Mach number, obtained from the flight data by using equation (7), for the flexible airplane are plotted in figure 12 for the three test altitudes of 15,000, 25,000, and 35,000 feet. Also plotted in figure 12 are calculated values of C_{L_β} and C_{L_δ} for the flexible airplane as obtained from equations (3) and (4) by using the rigid theoretical values of $\left(C_{L_\beta}\right)_{rigid}$ and $\left(C_{L_\delta}\right)_{rigid}$ from figure 11 and by substituting the value of S_v for S_v'. In all cases, it is seen that theory adequately predicted the flight parameters over the Mach number range. It is noted that the lift-curve slopes of the tail for the flexible-fuselage case showed little if any tendency to increase with Mach number, although there was an increase in the vertical-tail lift-curve slope of a nonswept tail on a straight-wing jet-bomber airplane presented in reference 10. This difference in variation of the lift-curve slope with Mach number was attributed mainly to the fuselage-flexibility relieving effect on the vertical-tail load and the reduced compressibility effects of a swept surface.

The rudder-effectiveness factor C_{L_δ}/C_{l_β} or α_e/δ (fig. 13) was obtained from parameters C_{L_δ} and C_{L_β} derived from equation (7) and flight measurements made in right-rudder-step maneuvers at 35,000 feet.

Values of C_{L_δ} were derived independently of the least-squares method by analyzing vertical-tail loads measured in rudder-step and rudder-pulse maneuvers before an appreciable sideslip angle developed. For this purpose, the rudder-deflection shear-load component was defined as

$$L = C_{L_\delta} q S_v' \delta$$

so that

$$C_{L_\delta} = \frac{L}{\delta} qS_v' \tag{24}$$

In order to determine C_{L_δ} from equation (24), the rate of change of vertical-tail shear load with rudder angle is required. The rate for several rudder steps and a rudder-pulse maneuver made at 35,000 feet and a Mach number of 0.66 was obtained from figure 14 (a plot of rudder angle and vertical-tail shear loads measured prior to development of

appreciable sideslip). The slope of the curve faired through the data points was used in equation (24) to calculate the specific value of $C_{L_\delta} = 0.020$ which, in this case, is approximately equal to the least-squares value given in figure 12. Values of C_{L_δ} for other rudder-step and rudder-pulse maneuvers were found in a similar way by using equation (24) at other Mach numbers and altitudes and agreed with the least-squares values.

Tail-parameter check.- In order to find out how well the tail parameters represent loads on the vertical tail, the parameters obtained from the least-squares analysis on one run were used to compute shear, bending-moment, and torque loads of other runs by means of equations (7), (8), and (9) and the measured flight values of β, $\dot{\psi}$, and δ. As an example of this type of check, the quantities β, $\dot{\psi}$, and δ from rudder-step, rudder-pulse, and aileron-roll maneuvers given in figures 6, 7, and 8, respectively, and values of β and δ measured during a steady sideslip were used in equations (7), (8), and (9) to calculate shear, bending-moment, and torque loads on the vertical tail with the least-squares parameters derived from the rudder-step data of figure 6. In figures 15, 16, 17, and 18, the calculated quantities were compared with measured values for rudder-step, aileron-roll, rudder-pulse, and steady-sideslip maneuvers made at 25,000 feet at a Mach number of 0.66. In figure 19, the shear, bending-moment, and torque loads which were computed for the aileron-roll maneuver in figure 16 but with parameters calculated from the roll-maneuver data are compared with measured values.

Examples shown in figures 15 to 19 are typical of all runs analyzed and indicate that the computed-load values were in agreement with the measured ones. Thus, it is believed that equations (7), (8), and (9) express the vertical-tail shear, bending-moment, and torque loads and that the vertical-tail parameters derived from these equations adequately represent loads on the vertical tail for rudder-step, rudder-pulse, aileron-roll, and steady-sideslip maneuvers analyzed.

Center of pressure.- Centers of pressure of the vertical-tail sideslip and rudder-deflection load components were derived from equations (14), (15), (16), and (17) and are plotted against Mach number in figure 20 for the sideslip load component and, in figure 21 for the rudder-deflection load component. Centers of pressure for vertical-tail load components (figs. 20 and 21) are shown superimposed on a plan form of the tail in figure 22.

As can be seen from figure 20, the spanwise center of pressure for the sideslip load component remained effectively constant over the Mach number range at about 90 inches outboard of the root station, which is the 40-percent-span station and also the location of the mean aerodynamic chord. The chordwise center of pressure was located approximately

10 inches forward of the strain-gage reference station R_2 and corresponds to 18 percent of the mean aerodynamic chord.

Data for determining the centers of pressure given in figure 21 for the rudder-deflection load component were obtained only from rudder-step maneuvers. The parameters obtained from aileron-roll and rudder-pulse maneuvers, which were required in defining the center of pressure, were not reliable. The center of pressure of the rudder-deflection load was located approximately 50 inches behind station R_2, or 50 percent of the mean aerodynamic chord at 40 percent of the span.

Directional Control Effectiveness and Dynamic Overyaw

The angle of sideslip per degree of rudder deflection β/δ was obtained from flight measurements of sideslip and from rudder angles taken during steady-sideslip maneuvers. Measurements were taken when the airplane was in steady sideslip, and the directional control effectiveness was simply the ratio of sideslip angle to rudder angle β/δ. The ratio β/δ is shown in figure 23 plotted against Mach number. It can be seen that the ratio decreases with Mach number from a value of -0.9 at a Mach number of 0.49 to approximately -0.6 at a Mach number of 0.81.

The ratio of the initial maximum sideslip angle, which is reached in a rudder-step maneuver, to the sideslip angle, obtained in a steady sideslip for equal rudder deflections, is the dynamic-overyaw factor. A plot of dynamic-overyaw factors is given in figure 24. It was not always possible in rudder-step maneuvers to hold the initial control deflection until the maximum sideslip angle was reached. Therefore, the dynamic-overyaw factors of figure 24 were based on the average maximum rudder angle. None of the flight values of the dynamic-overyaw factor quite reached a value of 1.7 which, according to reference 2, was used in design.

Airplane Yawing-Moment Parameters

The yawing moment of inertia of the airplane was determined by use of equation (18). The rate of change of vertical-tail load with yawing acceleration (eq. (18)) was obtained from figure 25. Values shown in figure 25 are maximum ones that occurred early in rudder-step maneuvers at 35,000 and 25,000 feet and at Mach numbers up to 0.82; these values occurred before any appreciable angular velocity or sideslip developed. Although the airplane weight varied from run to run by fuel consumptions, the approximate moment of inertia (I_Z = 2,400,000 lb-ft-sec^2) was calculated by substituting the slope $\frac{\partial L}{\partial \ddot{\psi}}$ of figure 25 into equation (18).

This value of I_Z is in close agreement with design values given in reference 2, when weight differences are considered.

The static directional stability contributed by the vertical tail in terms of the yawing-moment derivative $\left(C_{n_\beta}\right)_T$ was determined from equation (19) and plotted in figure 26 against Mach number. Flight values compare favorably with the design value of $\left(C_{n_\beta}\right)_T = 0.0035$ obtained from low-speed wind-tunnel tests in reference 9. Also shown in figure 26 are yawing-moment contributions resulting from rudder-deflection loads and which are obtained from equation (20). The design value of $C_{n_\delta} = 0.00148$ (refs. 2 and 9) enveloped the flight data for all test Mach numbers. The average flight value of C_{n_δ} was approximately 0.0013.

The yawing-moment derivative of the wing-fuselage combination $\left(C_{n_\beta}\right)_{WF}$ was determined from equation (21). Plotted in figure 27 are values of C_{n_β} derived from steady-sideslip measurements made at the three test altitudes. The derivatives remained effectively constant over the Mach number range. The average flight value of $\left(C_{n_\beta}\right)_{WF} = -0.0013$ (indicating directional instability) is seen to be in close agreement with the derived value from low-speed wind-tunnel data. (See refs. 9 and 11.)

Static directional-stability derivatives of the airplane $\left(C_{n_\beta}\right)_{WFT}$ were determined by two different methods (eqs. (22) and (23)) and are shown in figure 27. Values of $\left(C_{n_\beta}\right)_{WFT}$ obtained by the two methods were approximately of the same magnitude over the test Mach number and dynamic-pressure ranges. In applying equation (23), which sums the contributions of the wing-fuselage and tail yawing moments, an average value of $\left(C_{n_\beta}\right)_T = 0.0033$ was used. The low-speed wind-tunnel value of $\left(C_{n_\beta}\right)_{WFT} = 0.0021$ (ref. 11) is in good agreement with the flight values.

CONCLUSIONS

Vertical-tail lift-curve slopes obtained from flight data for the rigid-fuselage case compared favorably with theoretically derived values corrected for compressibility effects from low-speed wind-tunnel data.

Lift-curve slopes derived from sideslip load components for the flexible airplane remained effectively constant with Mach number at

35,000 feet and at lower altitudes showed a decrease with increasing Mach number; the variation in both instances was attributed to the relieving effect of fuselage flexibility. Agreement between flight values for the flexible airplane and theoretical values corrected for flexibility at the three test altitudes was good.

Flight values of the rudder lift-effectiveness factor did not increase with Mach number as the theoretical lift-effectiveness factors did but remained effectively constant. However, there was good agreement among the flight, design, and theoretical rudder lift-effectiveness factors.

Chordwise centers of pressure of the sideslip load components were located at approximately 18 percent of the mean aerodynamic chord and the rudder-deflection load-component centers of pressure were generally located at 50 percent of the mean aerodynamic chord for the test altitudes and Mach numbers. Spanwise centers of pressure of both load components were located at about 40 percent of the span (also the location of the mean aerodynamic chord).

The initial dynamic-overyaw sideslip angle reached after abruptly deflecting the rudder was approximately 1.5 times the sideslip angle reached in steady-sideslip maneuvers with equal rudder deflection. The directional-control effectiveness factor decreased from a value of -0.9 at a Mach number of 0.49 to a value of about -0.6 at a Mach number of 0.81.

Yawing-moment derivatives determined from the flight data were in agreement with design and wind-tunnel data. The wing-fuselage yawing-moment derivative indicated directional instability. The stability derivatives did not vary appreciably over the Mach number and dynamic-pressure ranges.

Langley Aeronautical Laboratory,
National Advisory Committee for Aeronautics,
Langley Field, Va., February 7, 1957.

REFERENCES

1. Skopinski, T. H., Aiken, William S., Jr., and Huston, Wilber B.: Calibration of Strain-Gage Installations in Aircraft Structures for the Measurement of Flight Loads. NACA Rep. 1178, 1954. (Supersedes NACA TN 2993.)

2. Gray, E. Z., Sandoz, P., and Entz, W.: Design Load Criteria. [Model B-47B.] Vol. I. Document No. D-9441 (Contract No. W33-038 ac-22413), Boeing Airplane Co., Nov. 9, 1948.

3. Bishop, Robert C., and Lomax, Harvard: A Simplified Method for Determining From Flight Data the Rate of Change of Yawing-Moment Coefficient With Sideslip. NACA TN 1076, 1946.

4. Pass, H. R.: Analysis of Wind-Tunnel Data on Directional Stability and Control. NACA TN 775, 1940.

5. DeYoung, John, and Harper, Charles W.: Theoretical Symmetric Span Loading at Subsonic Speeds for Wings Having Arbitrary Plan Form. NACA Rep. 921, 1948.

6. Murray, Harry E.: Wind-Tunnel Investigation of End-Plate Effects of Horizontal Tails on a Vertical Tail Compared With Available Theory. NACA TN 1050, 1946.

7. DeYoung, John: Theoretical Symmetric Span Loading Due to Flap Deflection for Wings of Arbitrary Plan Form at Subsonic Speeds. NACA Rep. 1071, 1952. (Supersedes NACA TN 2278.)

8. Abbott, Ira H., von Doenhoff, Albert E., and Stivers, Louis S., Jr.: Summary of Airfoil Data. NACA Rep. 824, 1945. (Supersedes NACA WR L-560.)

9. Ganzer, V. M., and Sandoz, Paul: Full Scale Test of the XB-47 Empennage. Part I - Analysis and Force Data. Document No. D-8517 (Contract No. W33-038 ac-8429), Boeing Airplane Co., Aug. 1947.

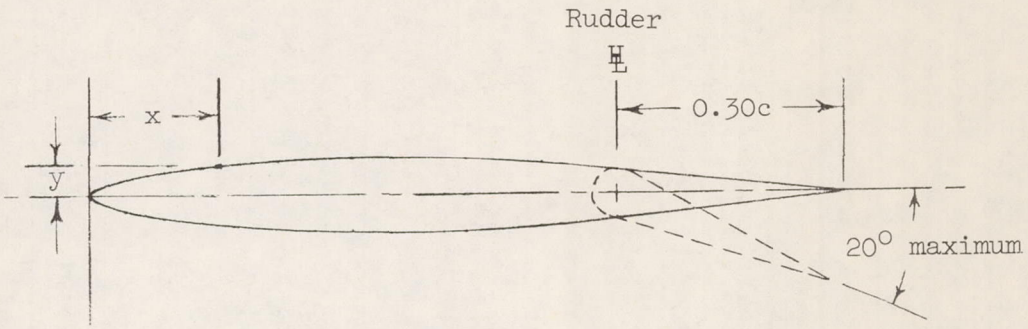
10. Cooney, T. V.: The Vertical-Tail Loads Measured During a Flight Investigation on a Jet-Powered Bomber Airplane. NACA RM L52G21, 1953.

11. Higgins, Paul R., and Budish, N. N.: Lateral Stability and Directional Control. Document No. D-8147, Boeing Airplane Co., Sept. 8, 1947.

TABLE I.- DIMENSIONS AND CHARACTERISTICS OF THE TEST AIRPLANE

Wing:	
Span, ft	116.0
Area, sq ft	1428.0
Aspect ratio	9.43
Taper ratio	0.42
Thickness ratio	0.12
Mean aerodynamic chord, in.	155.9
Sweep at 25-percent chord, deg	35.0
Root chord, in.	208.0
Tip chord, in.	87.0
Airfoil section	BAC 145
Incidence (root and tip), deg	2.75
Dihedral, deg	0
Horizontal tail:	
Span, ft	33.0
Area, sq ft	268
Aspect ratio	4.06
Taper ratio	0.42
Thickness ratio	0.10
Mean aerodynamic chord, in.	102.9
Sweep at 25-percent chord, deg	33.0
Root chord, in.	137.0
Tip chord, in.	58.0
Incidence, deg	-0.25
Airfoil section	BAC 100
Vertical tail:	
Span, ft	18.9
Area (including dorsal), sq ft	230.0
Area (outboard of strain-gage station), sq ft	182
Aspect ratio	1.55
Taper ratio	0.34
Thickness ratio	0.10
Mean aerodynamic chord, in.	158.4
Sweep at 25-percent chord, deg	35.0
Root chord, in.	216.0
Tip chord, in.	74
Airfoil section	BAC 100
Power plant:	
Six General Electric J-47-GE-23 turbojet engines with a sea-level miltary thrust rating of 5,800 pounds for each engine.	

TABLE II.- AIRFOIL ORDINATES OF VERTICAL TAIL



x (percent c)	y (percent c)	x (percent c)	y (percent c)
0	0	25.00	4.51
.50	.78	30.00	4.76
.75	.92	35.00	4.93
1.25	1.16	40.00	5.00
2.50	1.56	50.00	4.80
5.00	2.17	60.00	4.12
7.50	2.64	70.00	3.14
10.00	3.04	80.00	2.10
15.00	3.67	90.00	1.05
20.00	4.15	100.00	0

Airfoil section: 10-percent-thick BAC 100 section similar in cross section to the NACA 65-010 airfoil section modified with straight trailing edges rearward of the 66.5-percent chord.

TABLE III.- CHARACTERISTICS OF THE MANEUVERS ANALYZED

Flight	Run	Type of maneuver	Altitude, ft	Mach number	Airplane weight, lb	Center of gravity, percent of $\bar{c}$	l, ft
24	10	Right rudder step	34,400	0.60	110,000	23.3	52.5
24	16	Right rudder step	35,100	.66	109,000	22.8	52.6
24	17	Left rudder step	35,400	.66	109,000	22.8	52.6
24	22	Right rudder step	35,400	.71	108,000	23.9	52.4
24	27	Right rudder step	35,800	.77	108,000	22.8	52.6
24	32	Right rudder step	35,800	.82	107,000	22.8	52.6
24	41	Right rudder step	25,500	.65	104,000	23.8	52.4
24	42	Left rudder step	25,600	.66	104,000	24.0	52.4
27	11	Right rudder step	34,900	.66	110,000	21.2	52.7
27	12	Left rudder step	34,800	.67	110,000	21.2	52.7
26	9	Right rudder pulse	25,500	.76	115,000	20.8	52.8
26	15	Right rudder pulse	26,100	.71	114,000	20.3	52.8
26	22	Right rudder pulse	25,100	.60	112,000	20.4	52.8
26	28	Right rudder pulse	24,900	.54	111,000	20.2	52.9
26	30	Right rudder pulse	24,400	.49	110,000	19.6	53.0
27	6	Right rudder pulse	25,000	.70	117,000	28.4	51.8
27	7	Right rudder pulse	24,600	.65	117,000	28.4	51.8
27	8	Right rudder pulse	35,000	.82	112,000	20.8	52.8
27	9	Right rudder pulse	34,500	.71	111,000	20.8	52.8
27	10	Right rudder pulse	34,400	.66	111,000	21.1	52.7
27	36	Left rudder pulse	24,900	.66	106,000	21.0	52.7
28	22	Right rudder pulse	25,000	.49	114,000	21.4	52.7
28	23	Right rudder pulse	24,900	.49	114,000	21.4	52.7
28	26	Right rudder pulse	24,600	.61	114,000	21.6	52.7
28	27	Right rudder pulse	24,900	.60	114,000	21.7	52.6
28	30	Right rudder pulse	25,200	.71	113,000	21.7	52.6
28	31	Right rudder pulse	25,300	.70	113,000	21.7	52.6
28	37	Right rudder pulse	15,000	.49	112,000	21.5	52.7
28	43	Right rudder pulse	14,500	.60	111,000	21.4	52.7
28	45	Right rudder pulse	15,000	.70	110,000	20.3	52.9
24	9	Right aileron roll	34,600	.61	110,000	23.2	52.5
24	14	Right aileron roll	34,300	.66	109,000	22.9	52.6
24	15	Left aileron roll	34,700	.66	109,000	22.8	52.6
24	21	Right aileron roll	35,000	.72	109,000	22.9	52.6
24	26	Right aileron roll	35,700	.77	108,000	23.0	52.5
24	31	Right aileron roll	35,400	.82	107,000	22.6	52.6
24	39	Right aileron roll	24,900	.66	105,000	23.3	52.5
26	8	Right aileron roll	24,900	.76	115,000	21.1	52.7
26	10	Right aileron roll	25,000	.70	115,000	21.1	52.7
26	16	Right aileron roll	24,700	.65	113,000	20.5	52.8
26	17	Right aileron roll	24,700	.60	113,000	20.2	52.9
26	23	Right aileron roll	24,700	.55	112,000	20.5	52.8
26	29	Right aileron roll	24,700	.49	111,000	19.8	52.9
26	31	Right aileron roll	15,000	.59	110,000	19.6	53.0
26	32	Left aileron roll	14,800	.58	110,000	19.6	53.0
27	37	Right aileron roll	14,700	.49	105,000	21.0	52.7
27	38	Right aileron roll	14,600	.70	105,000	20.8	52.8
24	11,12,13	Left steady sideslip	34,000	.59	110,000	23.2	52.5
24	18,19,20	Left steady sideslip	35,400	.66	109,000	22.9	52.6
24	23,24,25	Left steady sideslip	35,900	.72	108,000	22.9	52.6
24	28,29,30	Left steady sideslip	36,000	.77	108,000	22.8	52.6
24	33,34,35	Left steady sideslip	37,500	.81	107,000	22.6	52.6
24	43,44,45	Left steady sideslip	25,400	.66	104,000	24.2	52.4
24	46,47	Right steady sideslip	25,400	.66	104,000	24.2	52.4
26	11,12,13,14	Left steady sideslip	25,800	.70	114,000	20.5	52.8
26	18,19,20,21	Left steady sideslip	25,000	.60	112,000	20.6	52.8
26	24,25,26,27	Left steady sideslip	24,900	.54	111,000	19.9	52.9
26	33,34,35	Left steady sideslip	15,500	.59	109,000	19.4	53.0
26	36,37	Right steady sideslip	15,500	.59	109,000	19.4	53.0
27	13,14,15,16	Left steady sideslip	24,700	.49	109,000	21.6	52.7
27	17,18,19,20	Left steady sideslip	25,100	.55	109,000	21.7	52.6
27	27,28,29,30	Left steady sideslip	25,700	.70	108,000	21.0	52.7
27	31,32,33,34	Left steady sideslip	25,600	.76	107,000	21.0	52.8
28	1,2,3,4,5	Left steady sideslip	34,700	.65	118,000	21.9	52.6
28	6,7,8,9,10	Left steady sideslip	34,700	.71	117,000	21.9	52.6
28	11,12,13,14,15	Left steady sideslip	34,900	.78	117,000	21.8	52.6
28	16,17,18,19,20	Left steady sideslip	34,900	.81	116,000	21.7	52.6
28	33,34,35,36	Left steady sideslip	14,700	.49	112,000	21.7	52.6
28	39,40,41,42	Left steady sideslip	14,900	.59	112,000	21.6	52.7

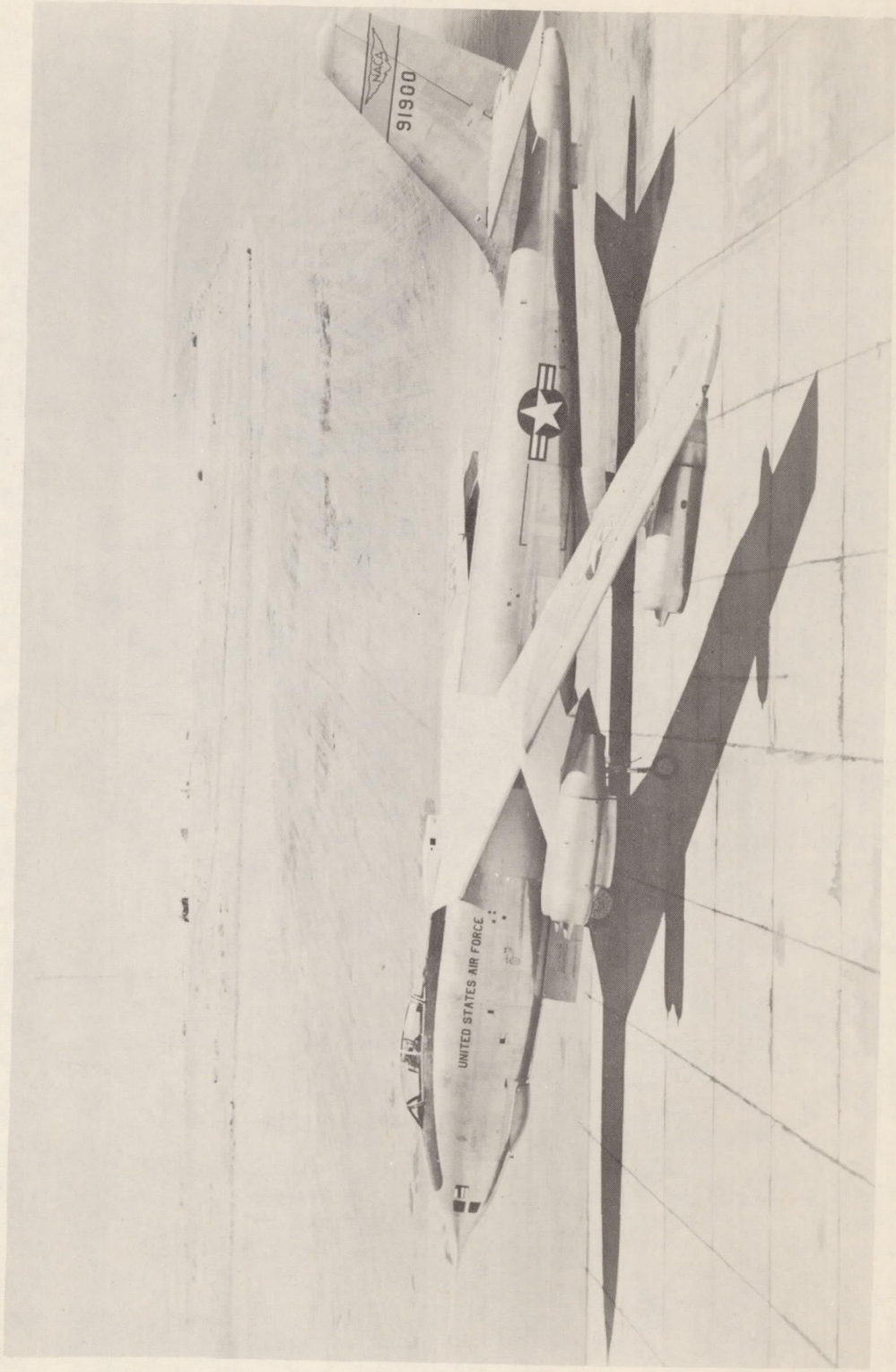


Figure 1.- Test airplane. L-86692

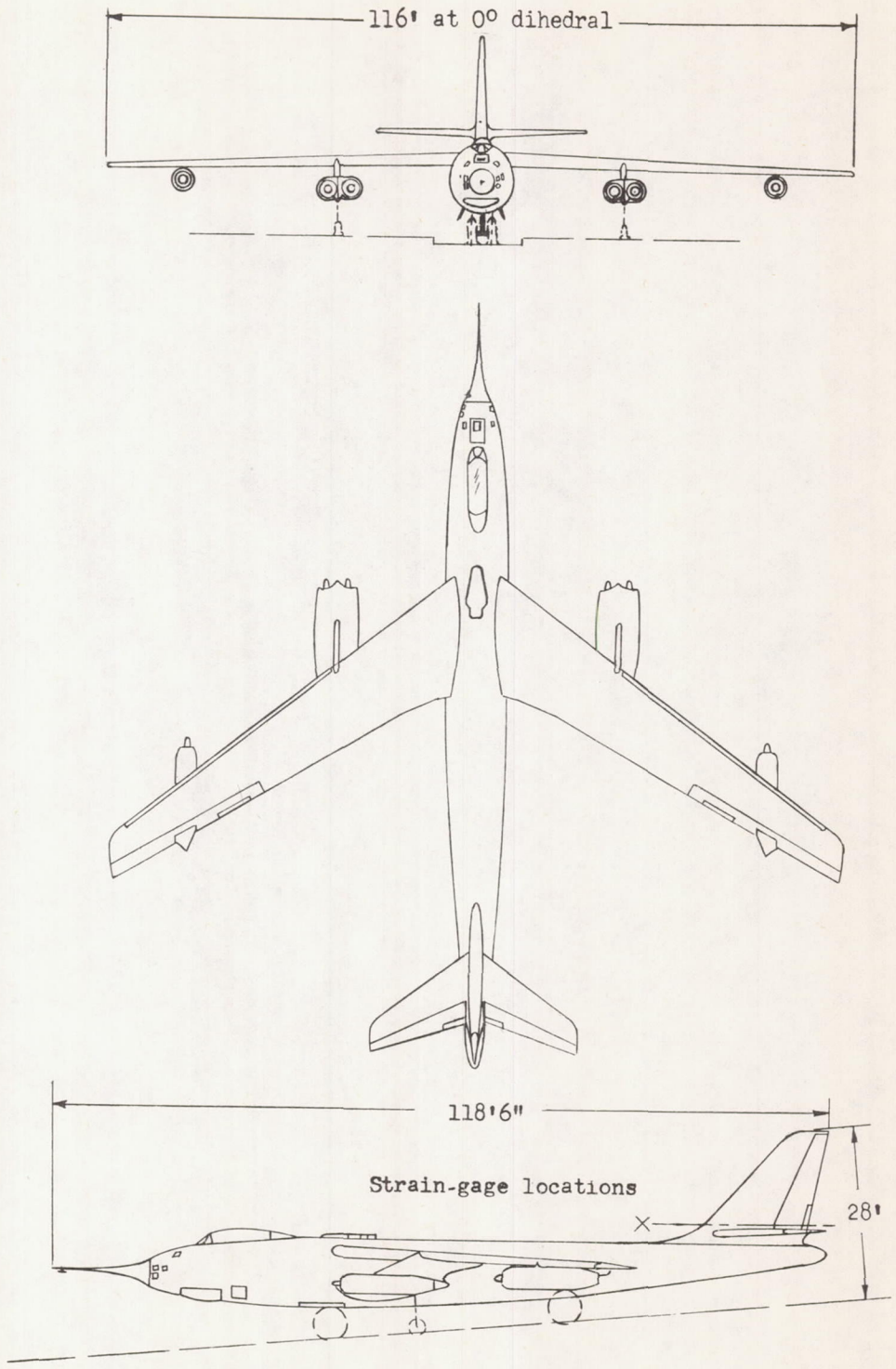


Figure 2.- Principal dimensions of the test airplane.

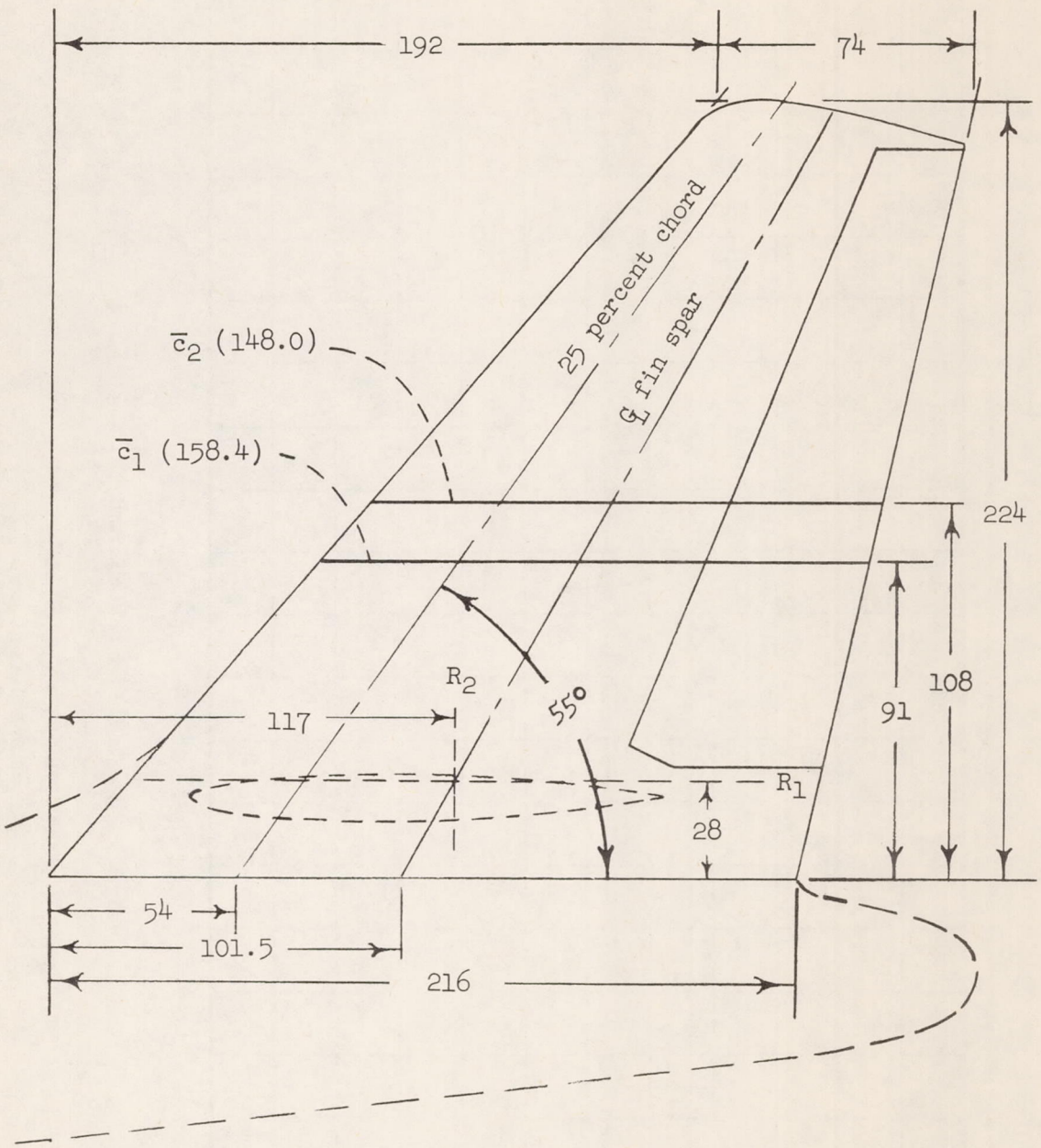


Figure 3.- Vertical tail. R_1 and R_2 are strain-gage reference axes. All dimensions are in inches.

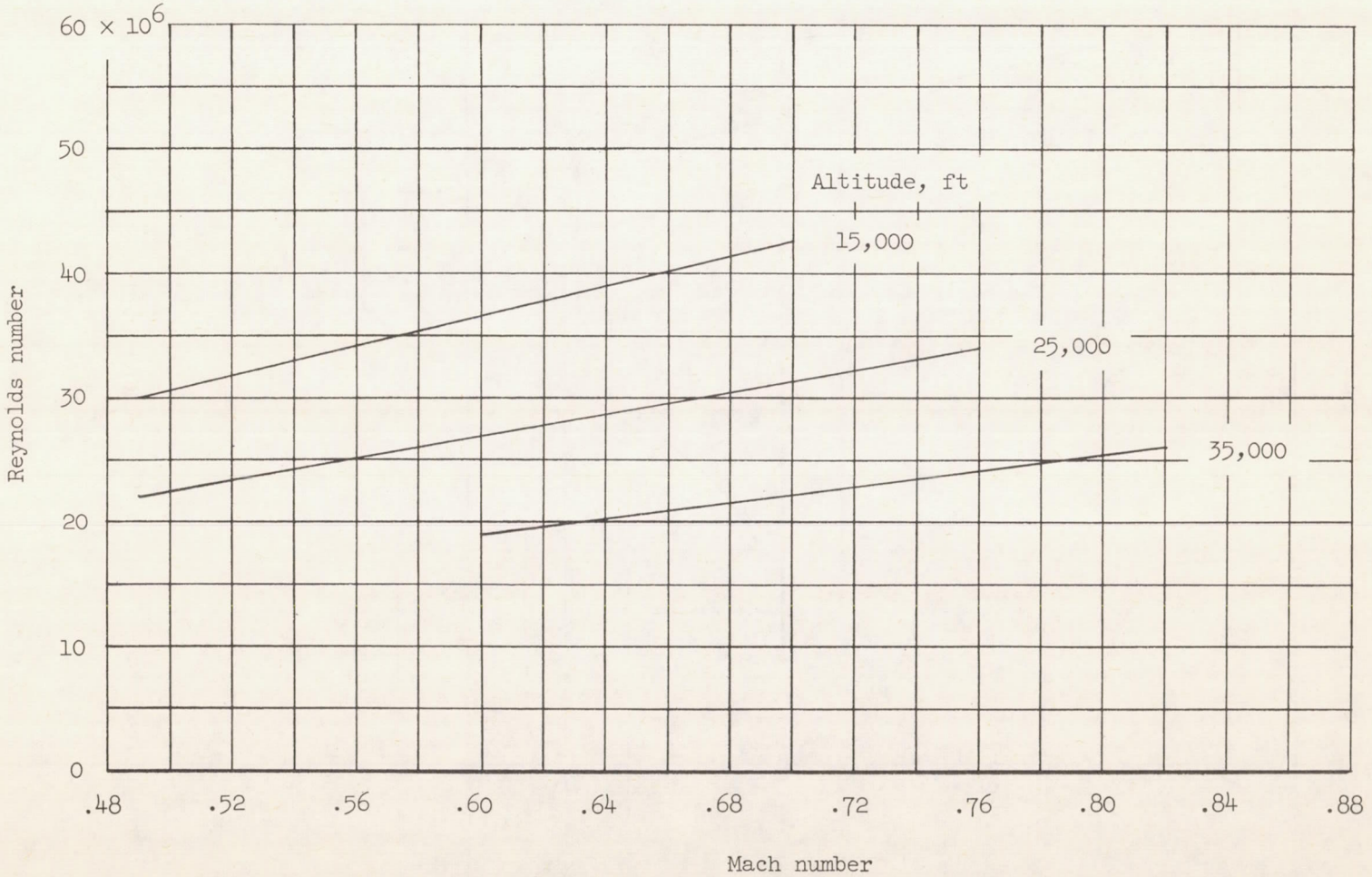


Figure 4.- Variation of Reynolds number with Mach number at the three test altitudes. Reynolds numbers based on $\bar{c}_1$.

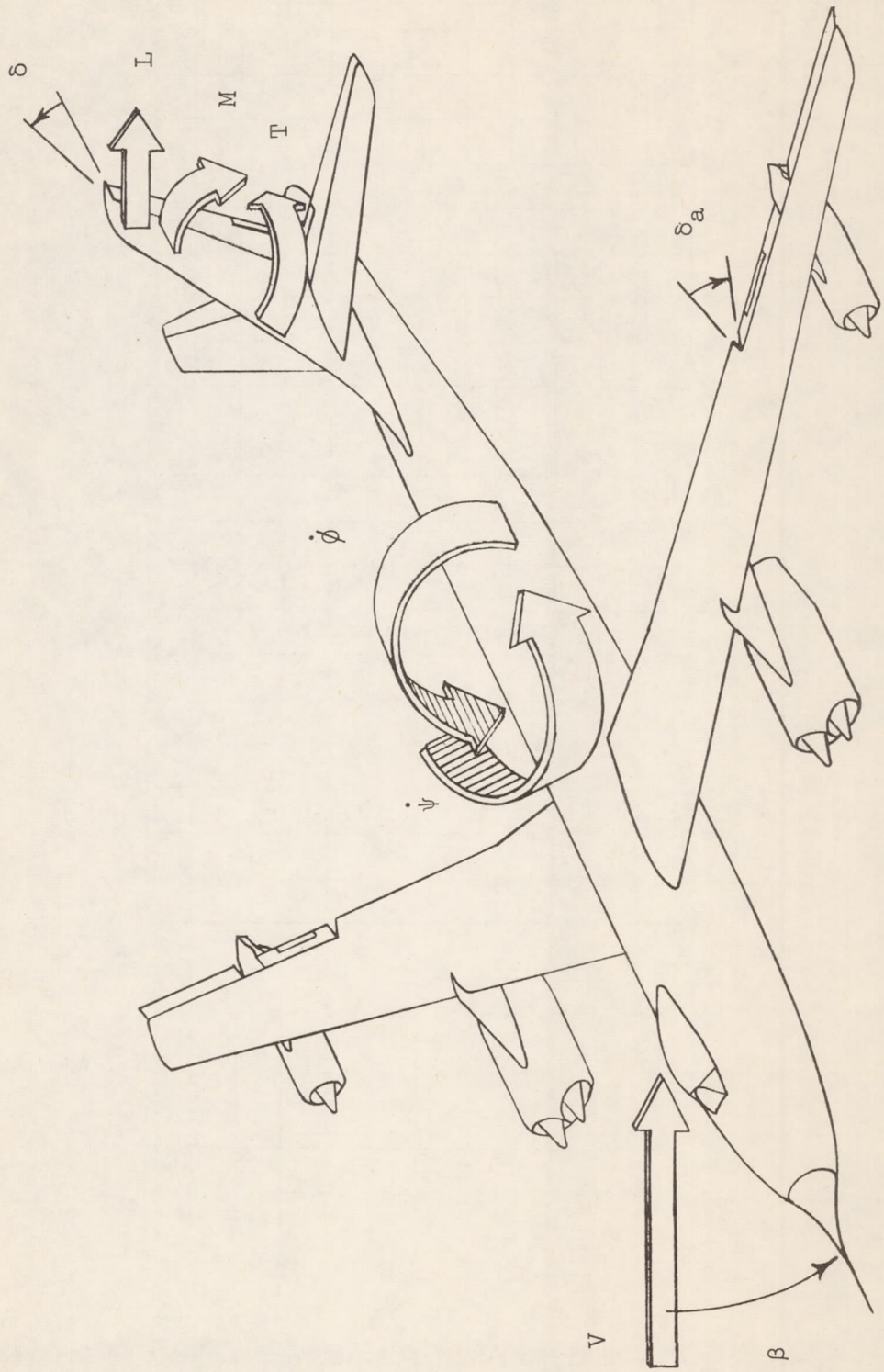


Figure 5.- Positive directions of measured quantities.

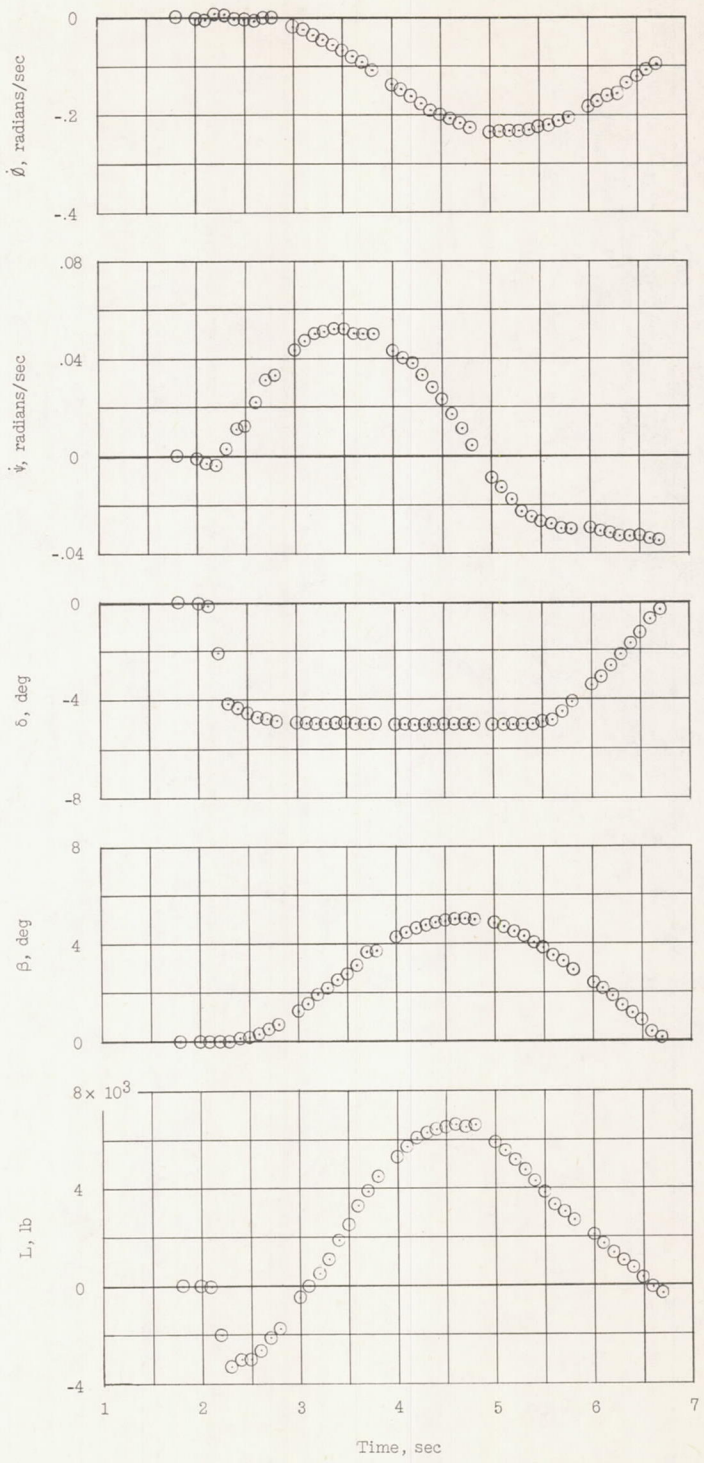


Figure 6.- Measured quantities during a left-rudder-step maneuver. Flight 24, run 42; $\delta_a = 0^\circ$.

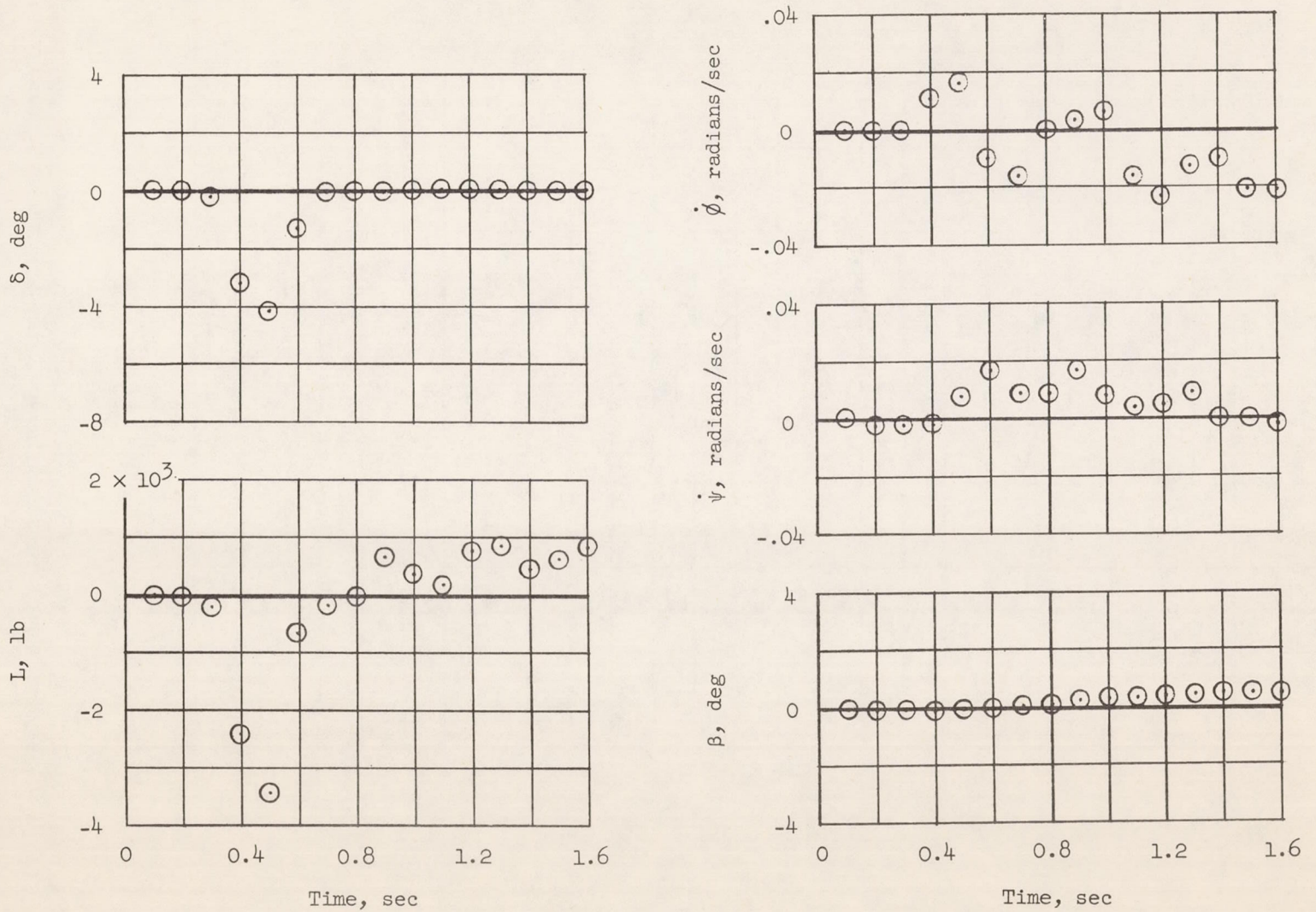


Figure 7.- Measured quantities during a left-rudder-pulse maneuver. Flight 27, run 36; $\delta_a = 0^o$.

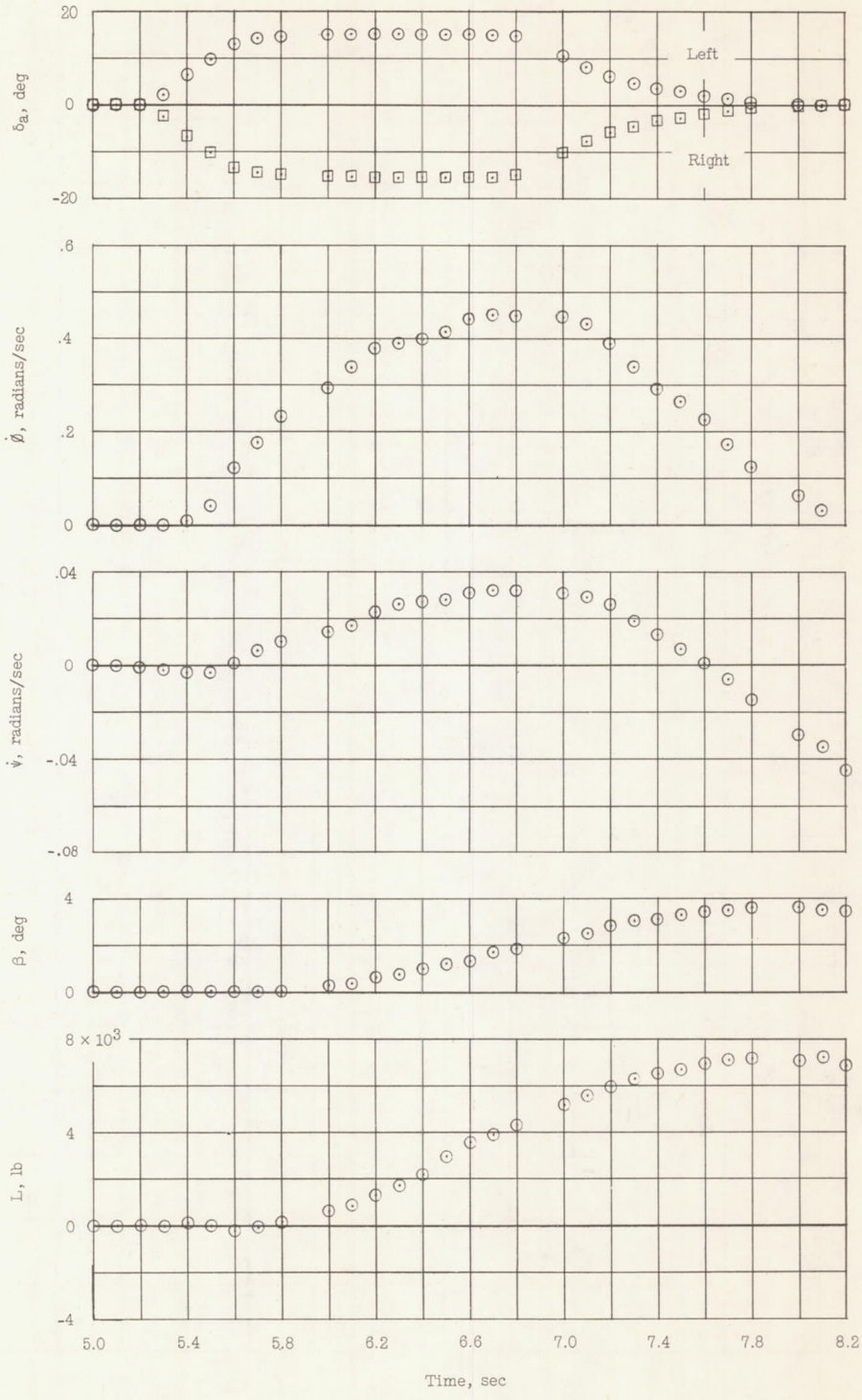


Figure 8.- Measured quantities during a right-aileron-roll maneuver. Flight 24, run 39; $\delta = 0^{o}$.

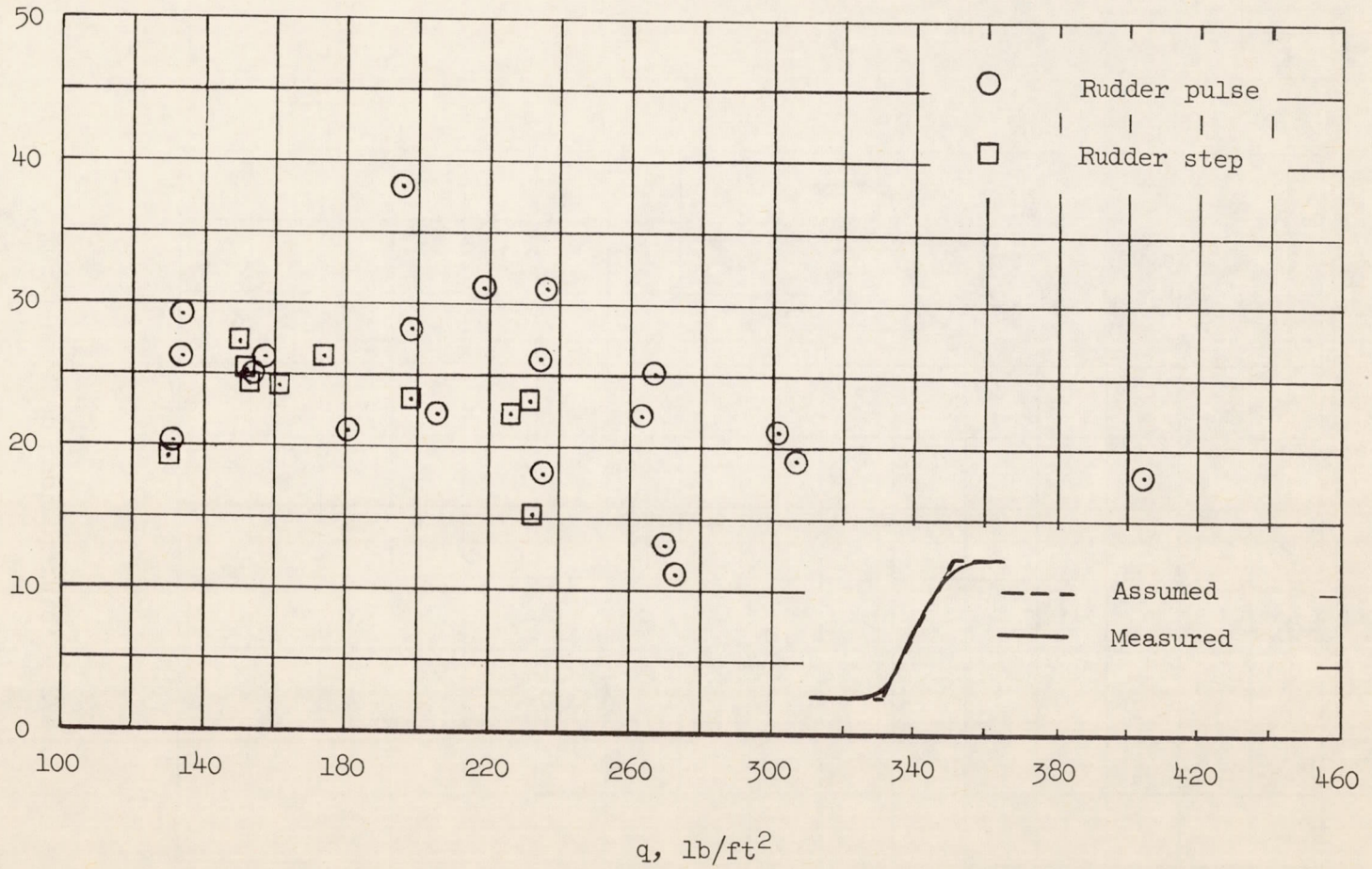


Figure 9.- Maximum control rates used in the rudder-step and rudder-pulse maneuvers.

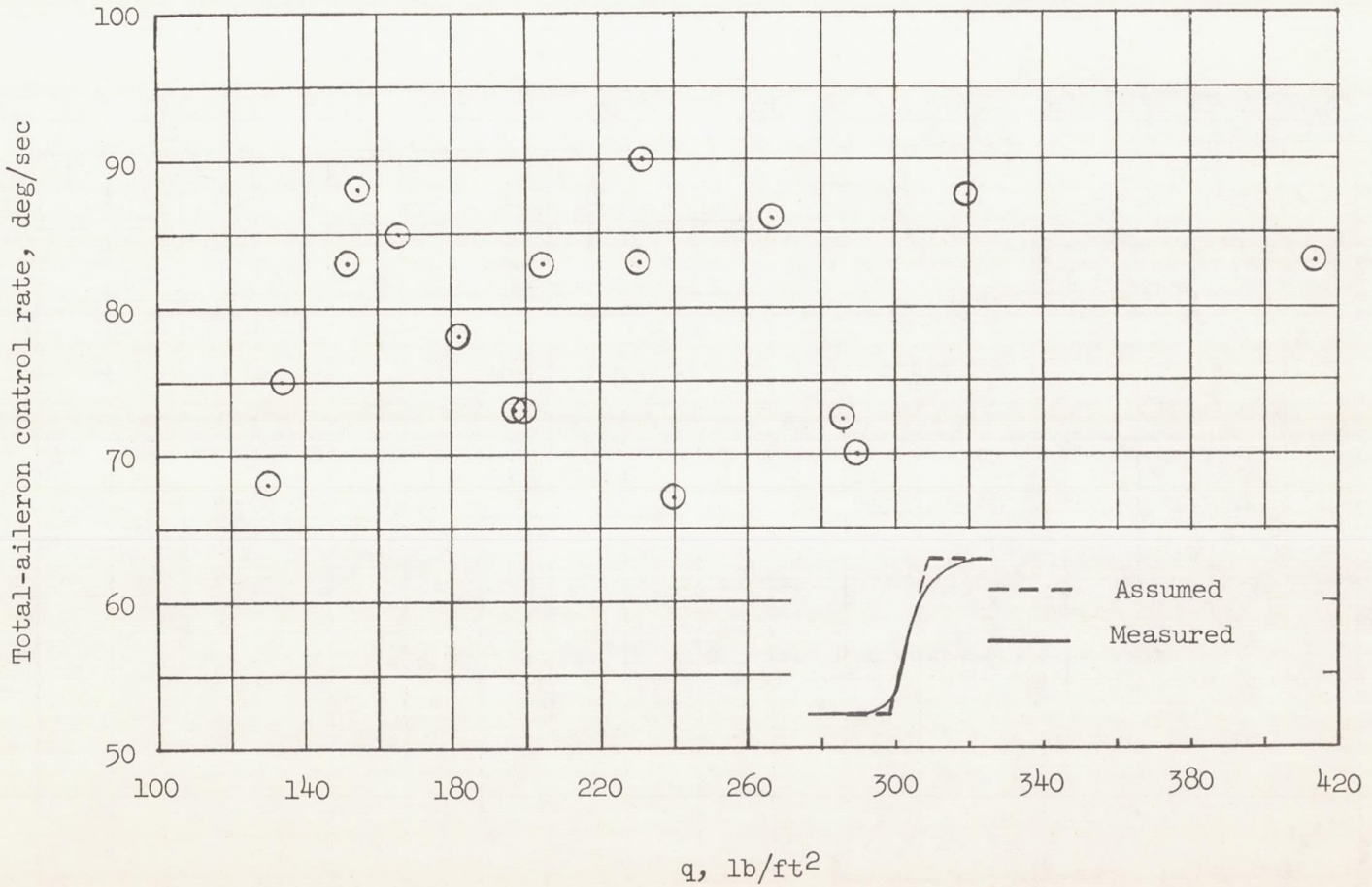


Figure 10.- Maximum total-aileron control rates used in the aileron-roll maneuvers.

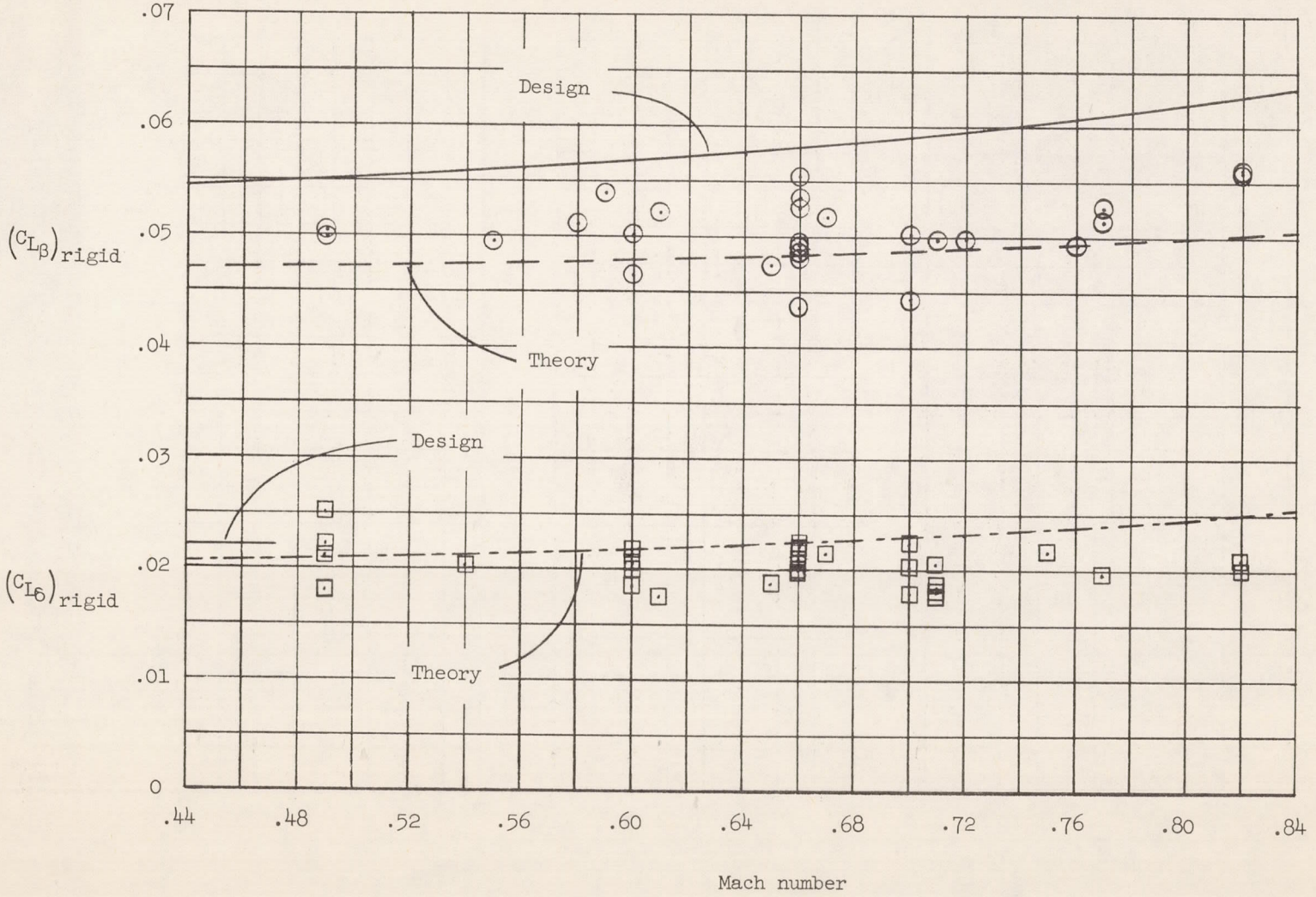


Figure 11.- Vertical-tail lift-curve slopes for the sideslip angle and rudder-deflection load components. Rigid fuselage.

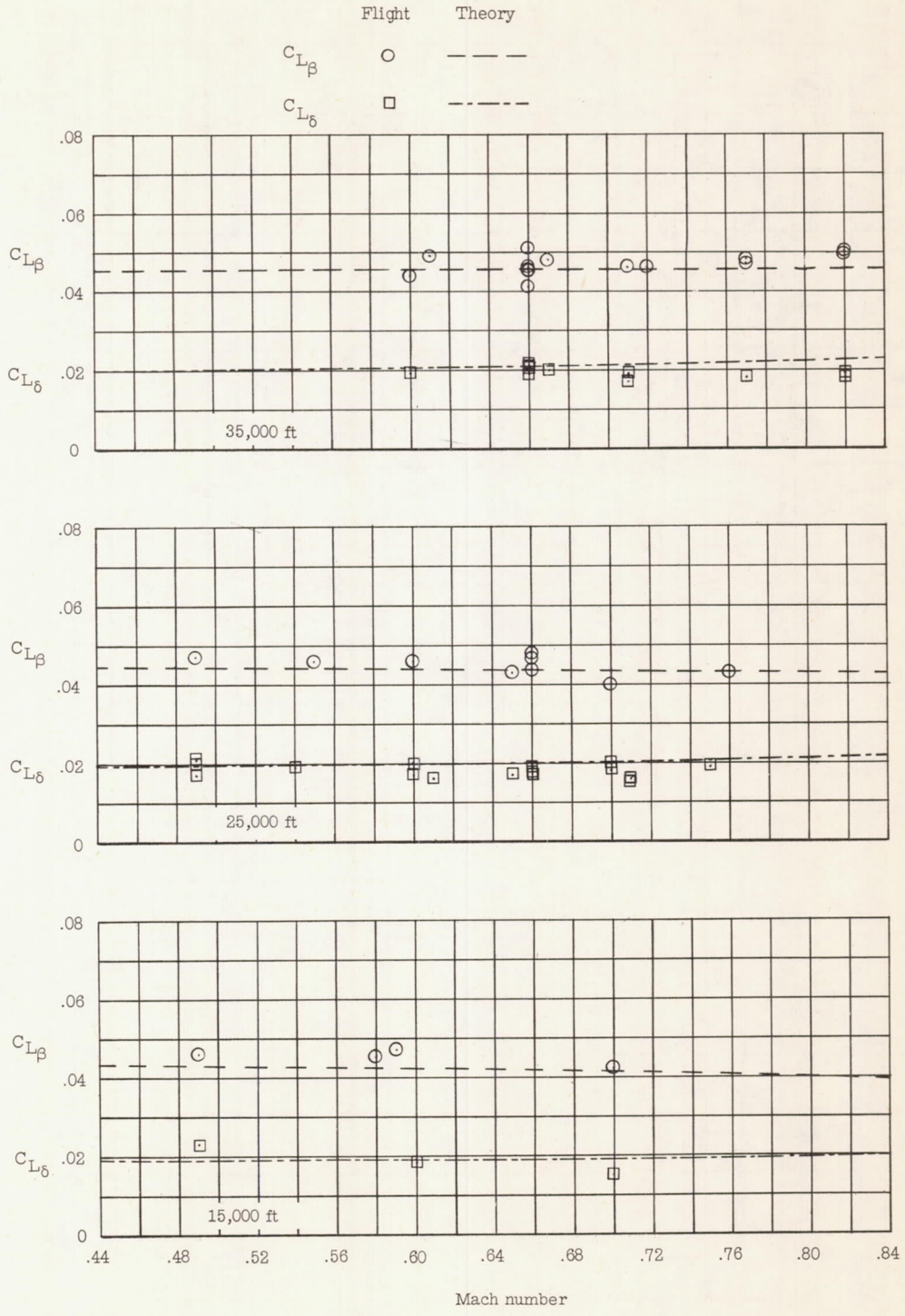


Figure 12.- Vertical-tail lift-curve slopes for the sideslip angle and rudder-deflection load components. Flexible fuselage.

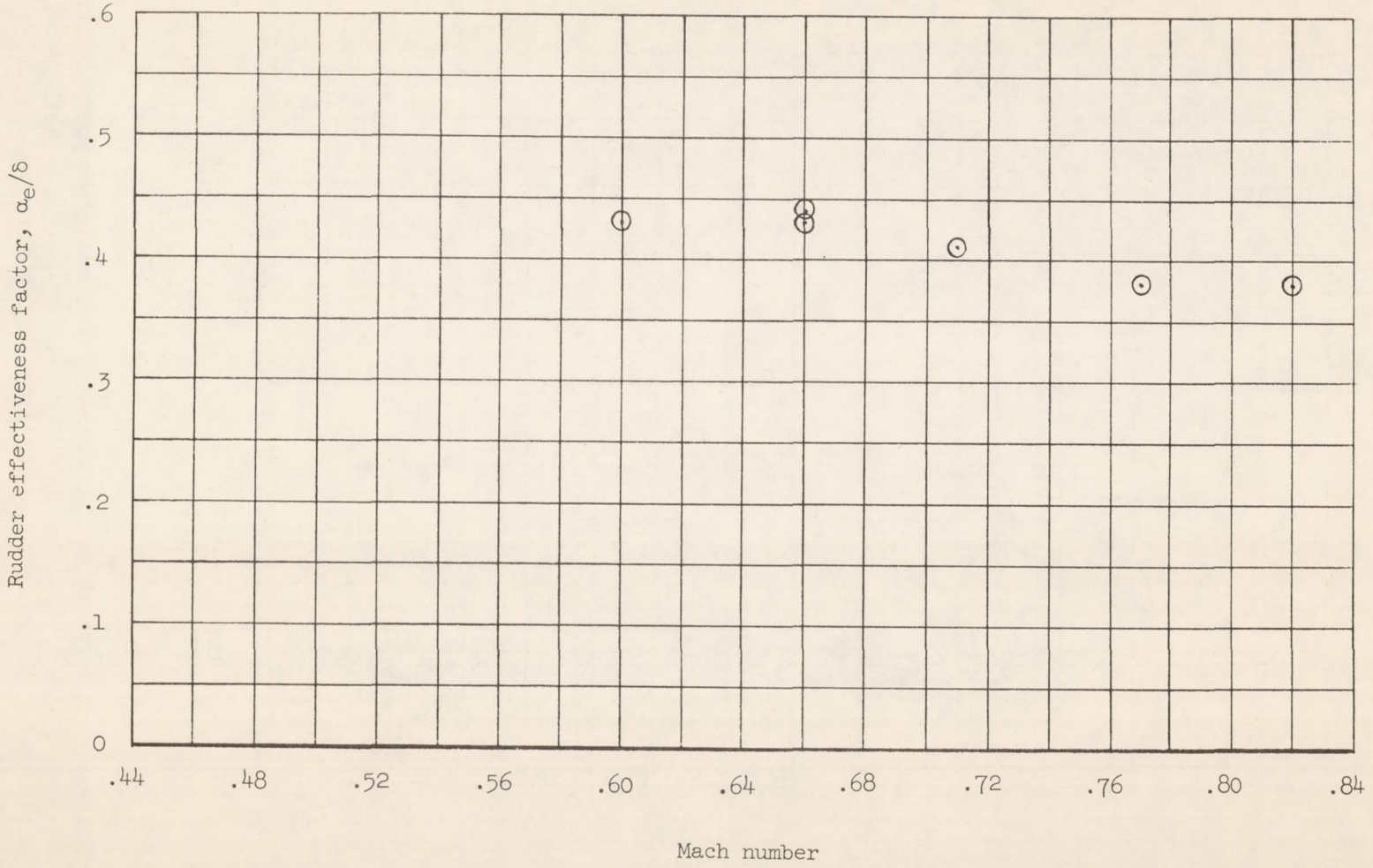


Figure 13.- Rudder effectiveness factor. Data were obtained from right-rudder-step maneuvers at 35,000 feet.

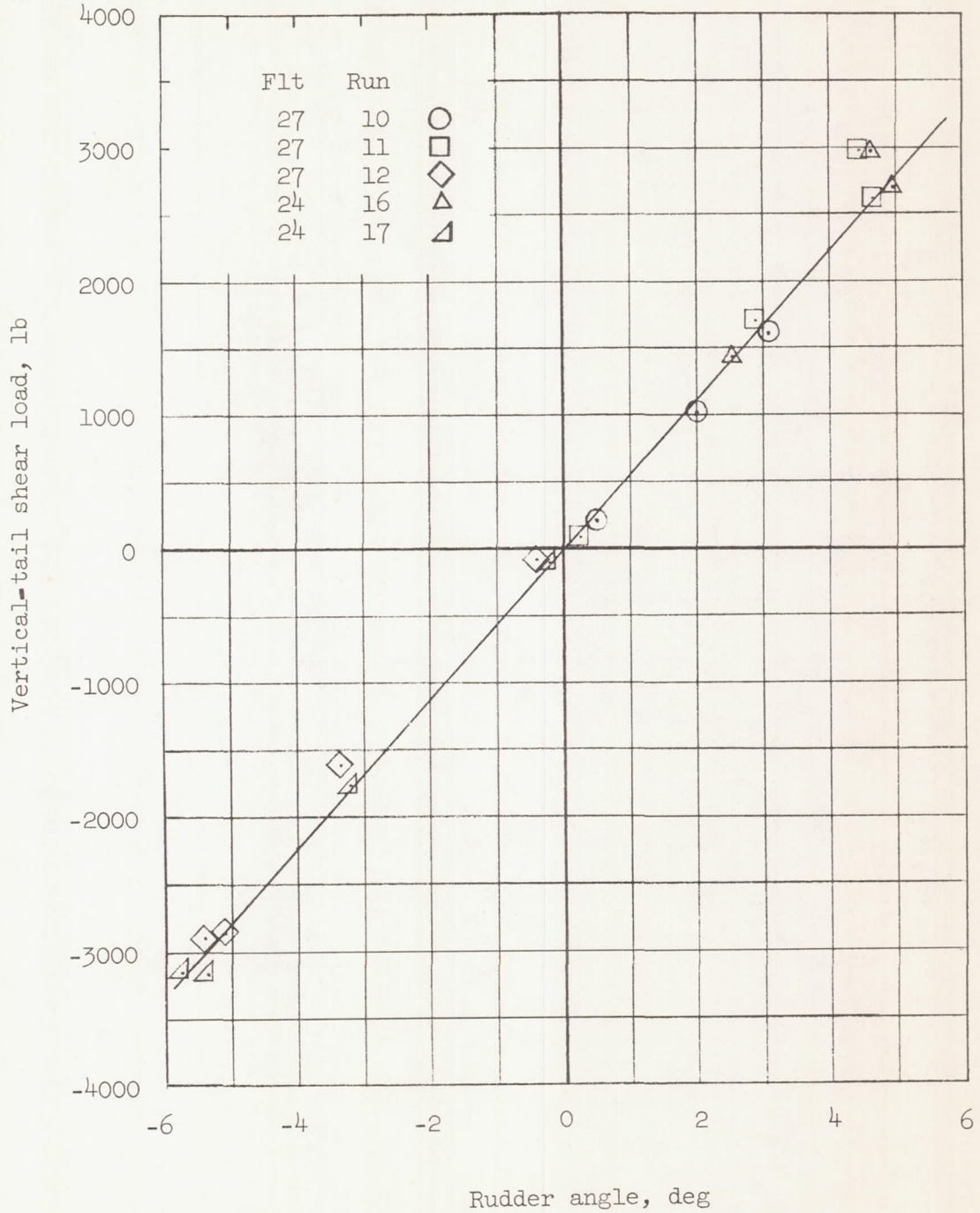


Figure 14.- Vertical-tail shear load measured in rudder-pulse and rudder-step maneuvers (prior to development of appreciable sideslip angle) at a Mach number of 0.66 and an altitude of 35,000 feet.

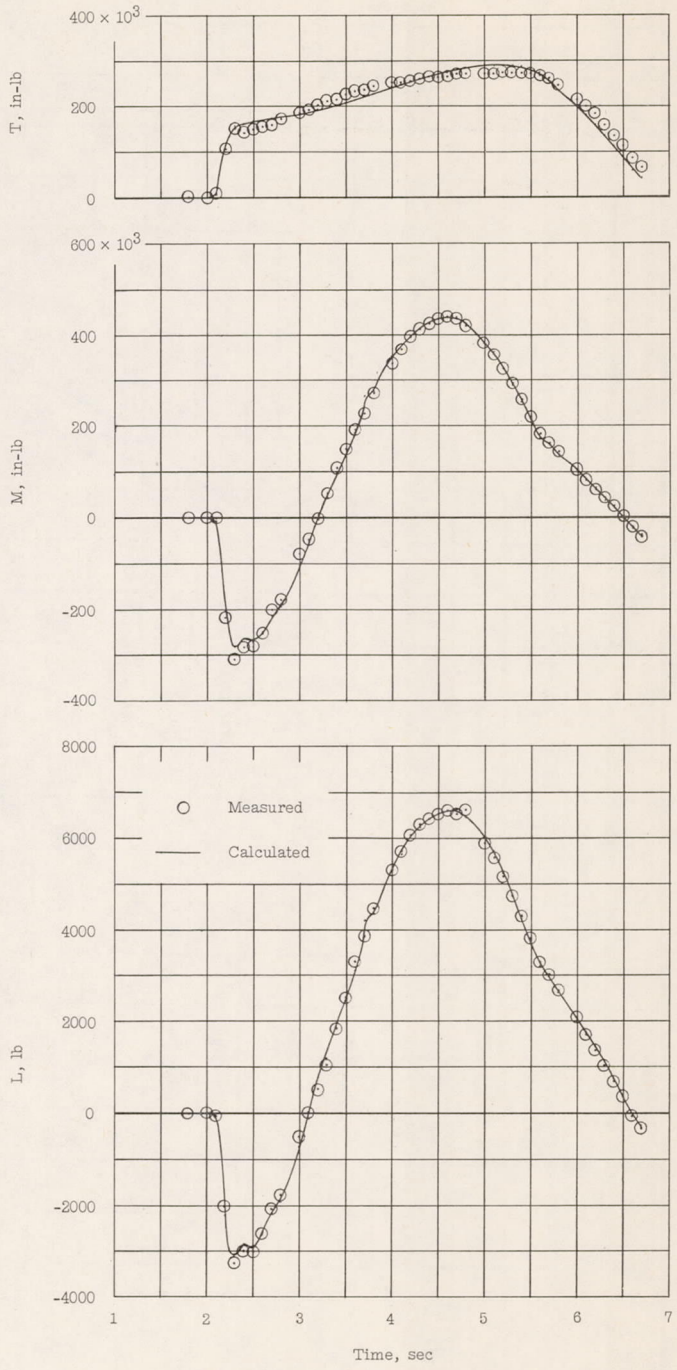


Figure 15.- Measured and calculated vertical-tail shear, bending-moment, and torque loads for a rudder-step maneuver at a Mach number of 0.66 and altitude of approximately 25,000 feet. Parameters used were determined from rudder-step maneuver.

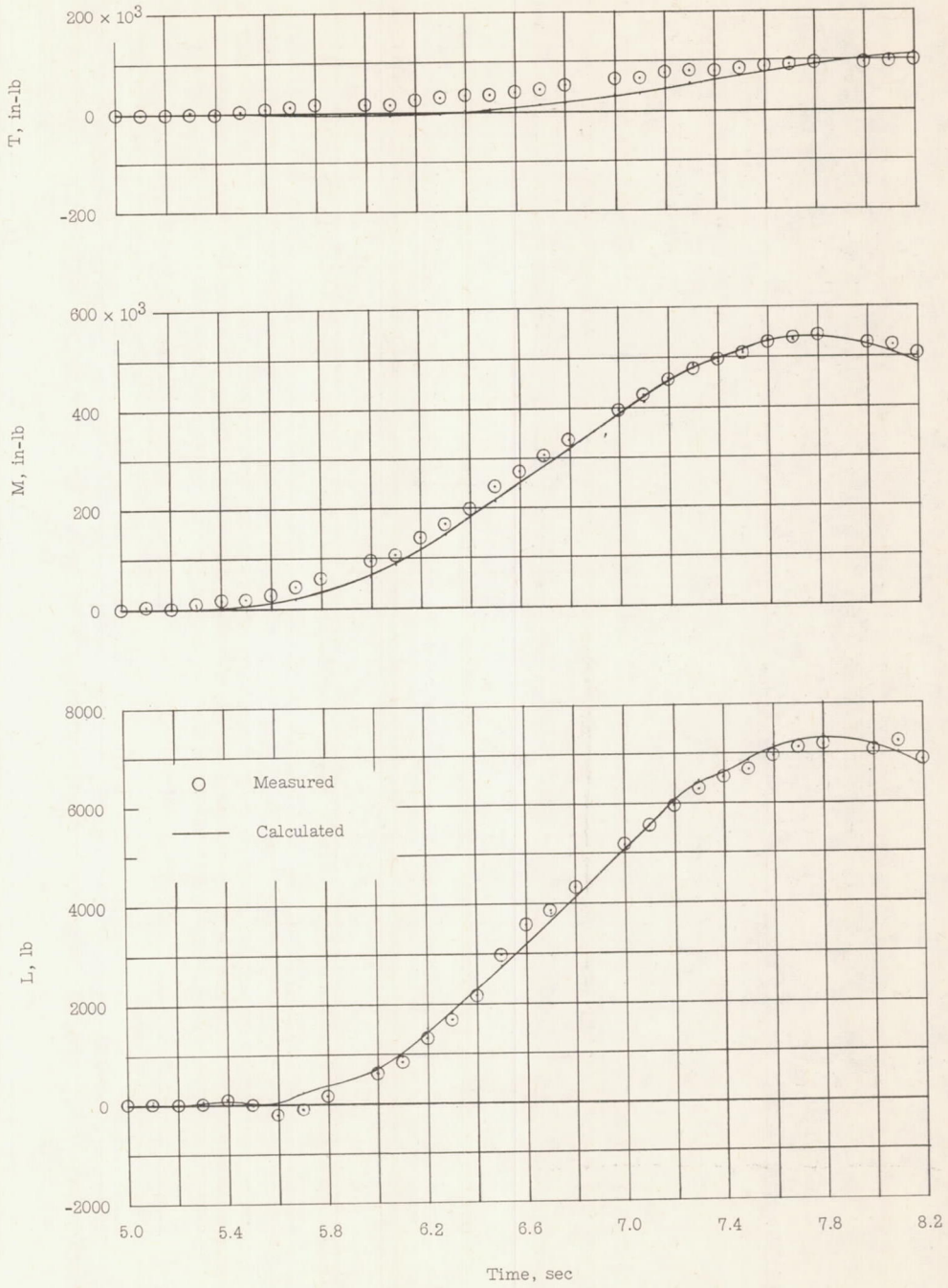


Figure 16.- Measured and calculated vertical-tail shear, bending-moment, and torque loads for an aileron-roll maneuver made at a Mach number of 0.66 and altitude of 25,000 feet. Parameters used were determined from a rudder-step maneuver.

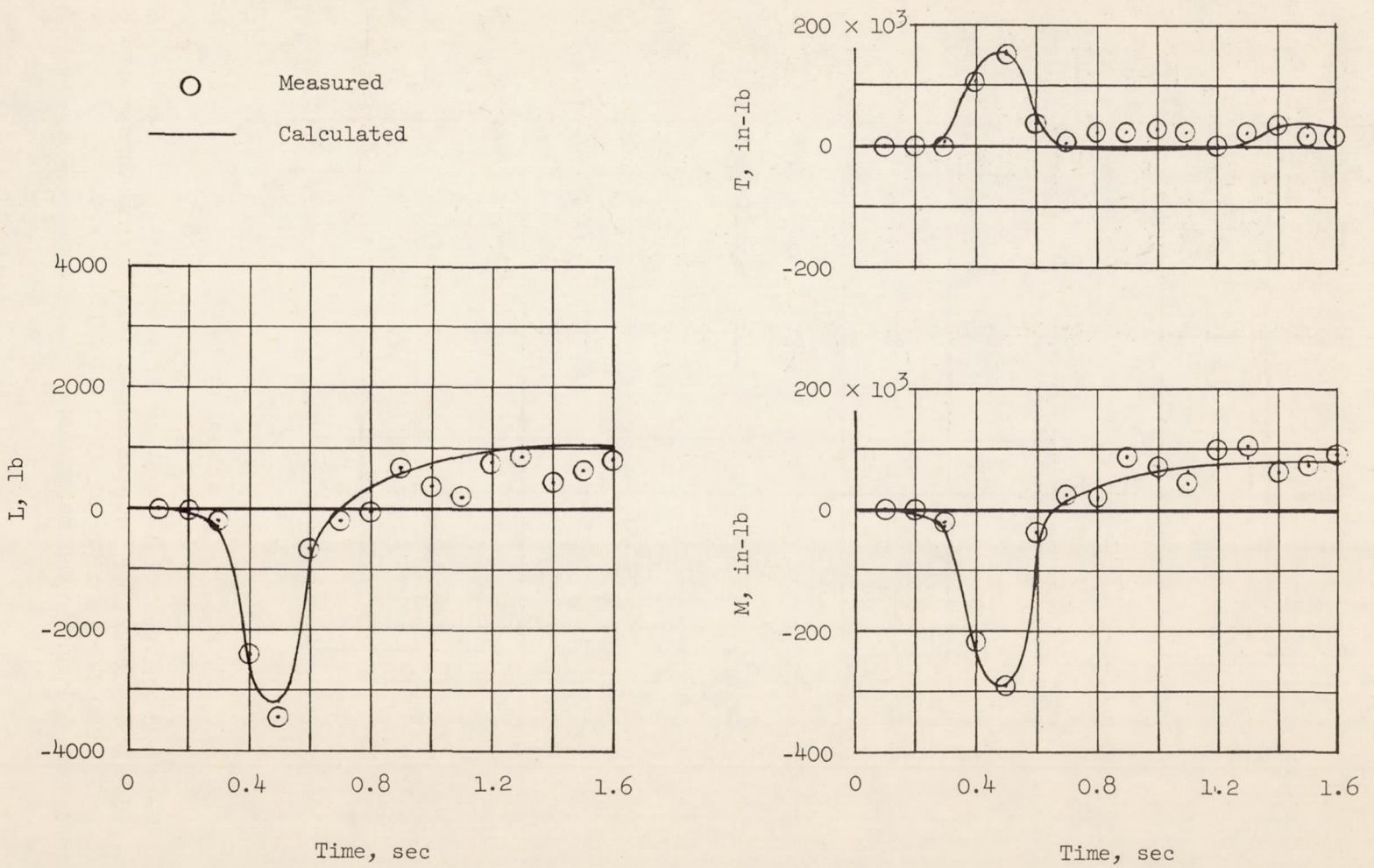


Figure 17.- Measured and calculated vertical-tail shear, bending-moment, and torque loads for a rudder-pulse maneuver made at a Mach number of 0.66 and altitude of 25,000 feet. Parameters used were determined from a rudder-step maneuver.

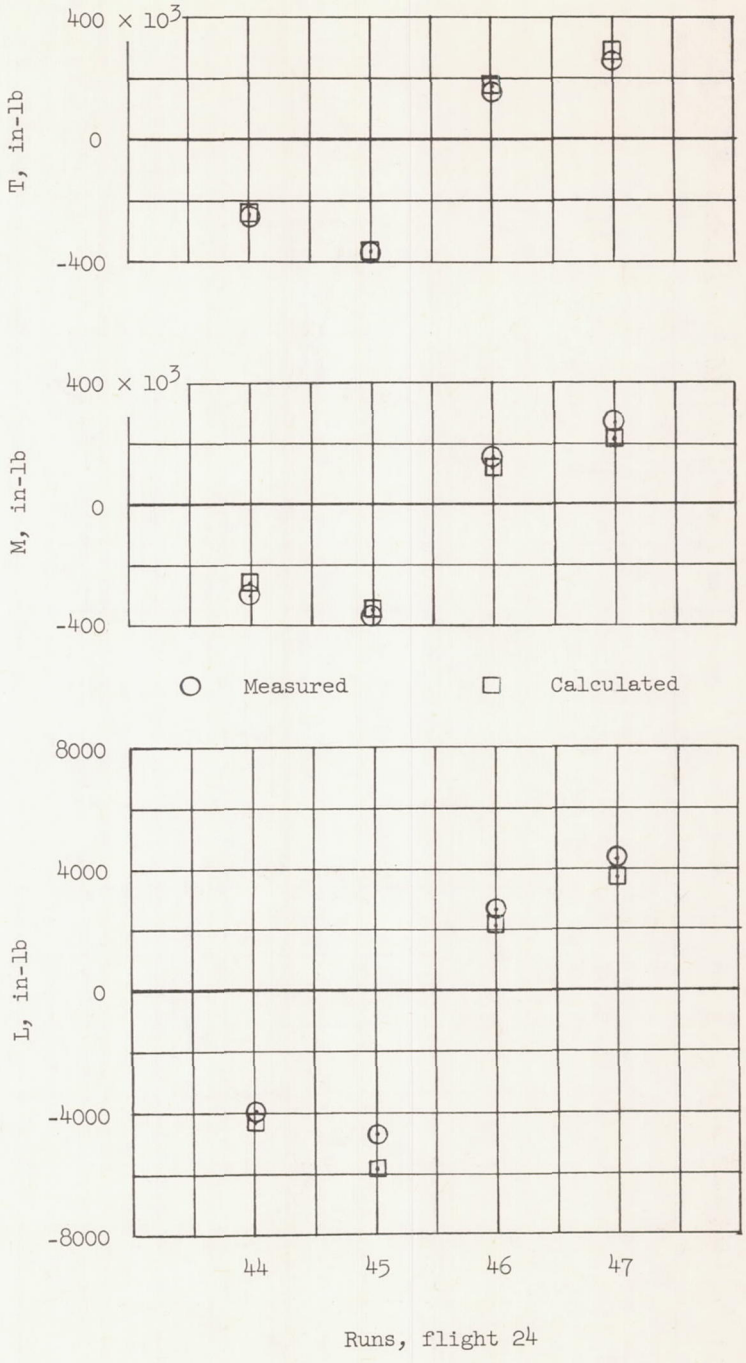


Figure 18.- Measured and calculated values of vertical-tail shear, bending-moment, and torque loads for four steady-sideslip maneuvers made at an altitude of 25,000 feet and Mach number of 0.66. Parameters used were determined from a rudder-step maneuver.

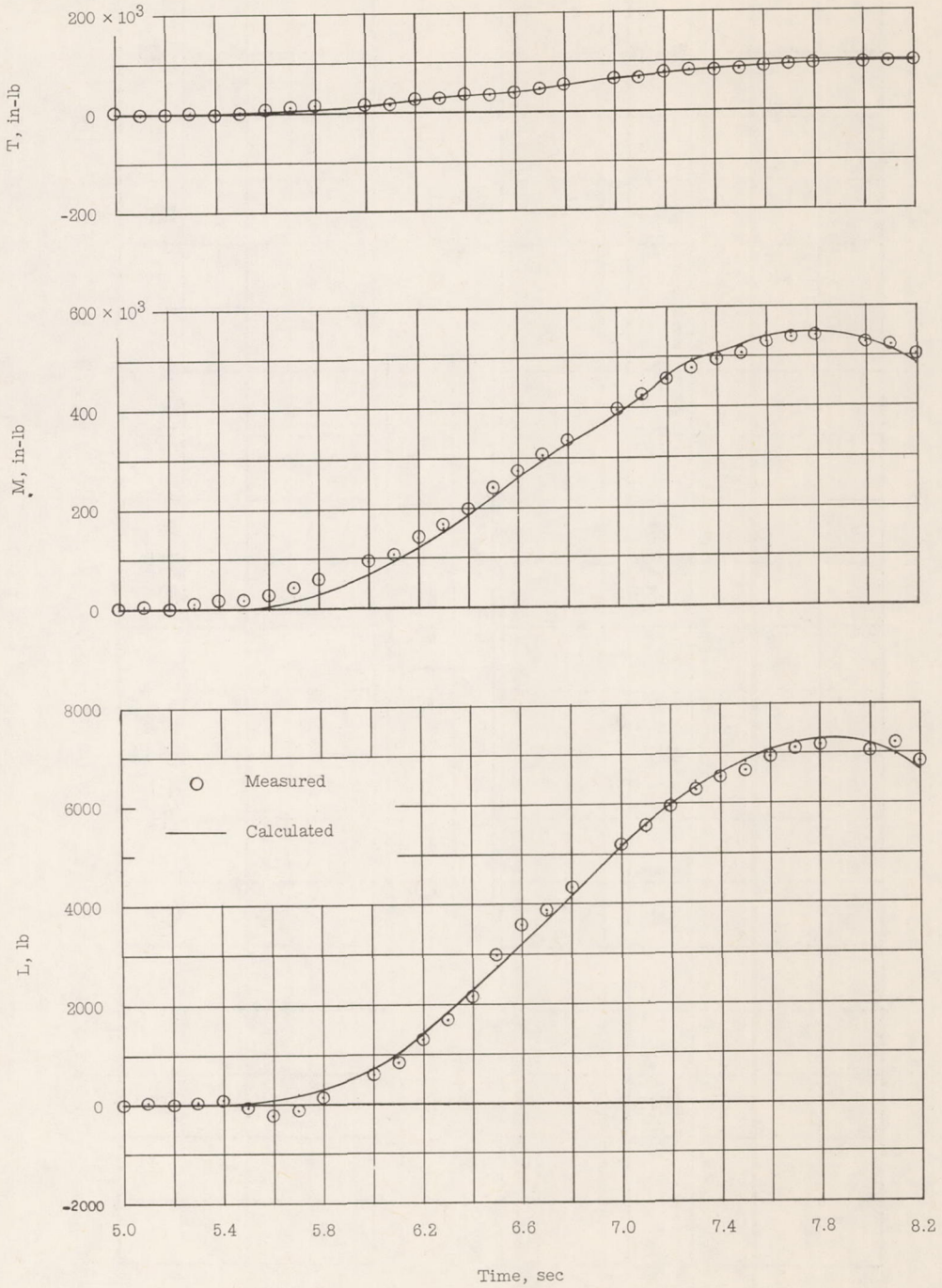


Figure 19.- Measured and calculated vertical-tail shear, bending-moment, and torque loads for an aileron-roll maneuver made at a Mach number of 0.66 and altitude of 25,000 feet. Parameters used were determined from the roll maneuver.

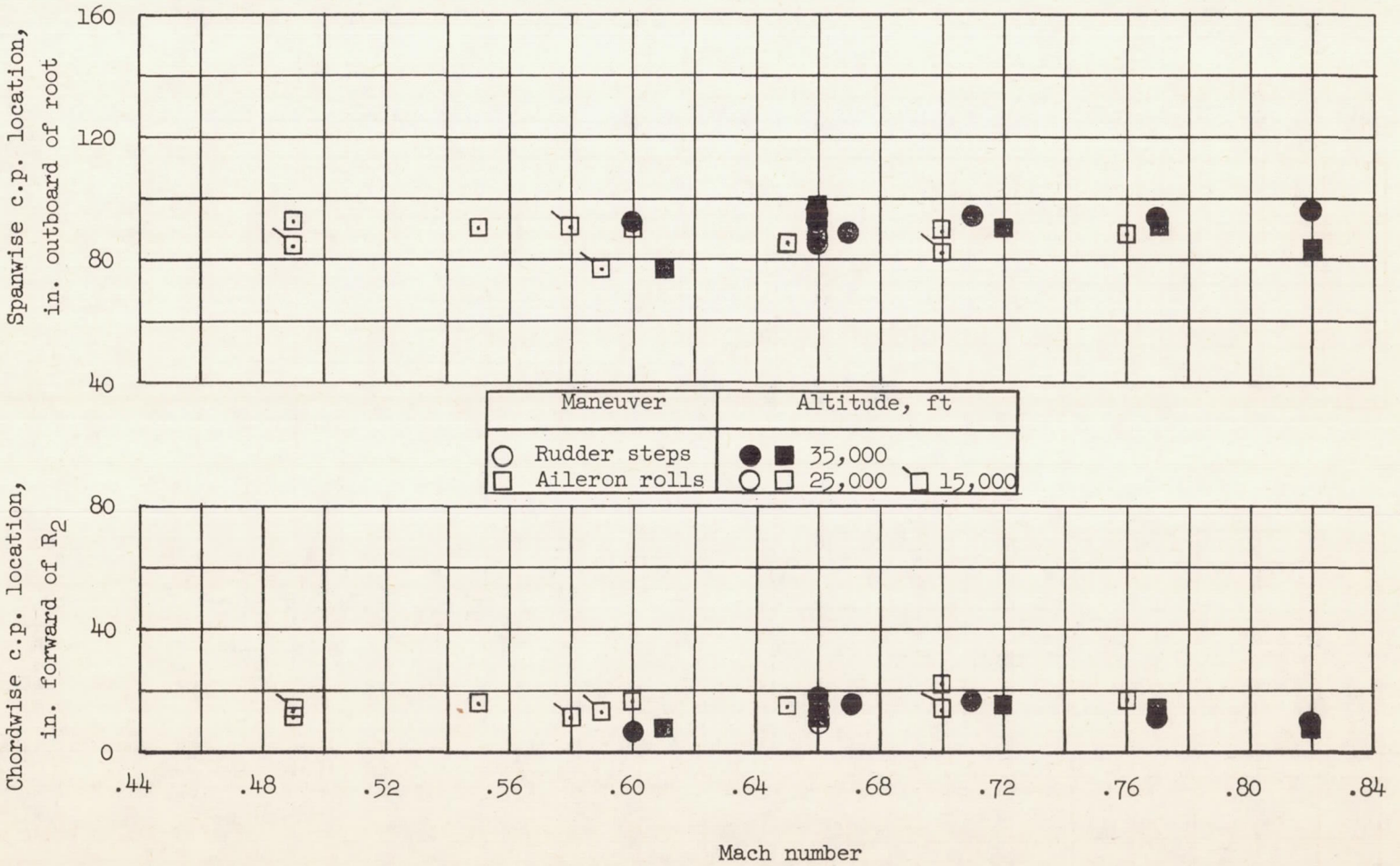


Figure 20.- Spanwise and chordwise center-of-pressure locations for the sideslip vertical-tail load component.

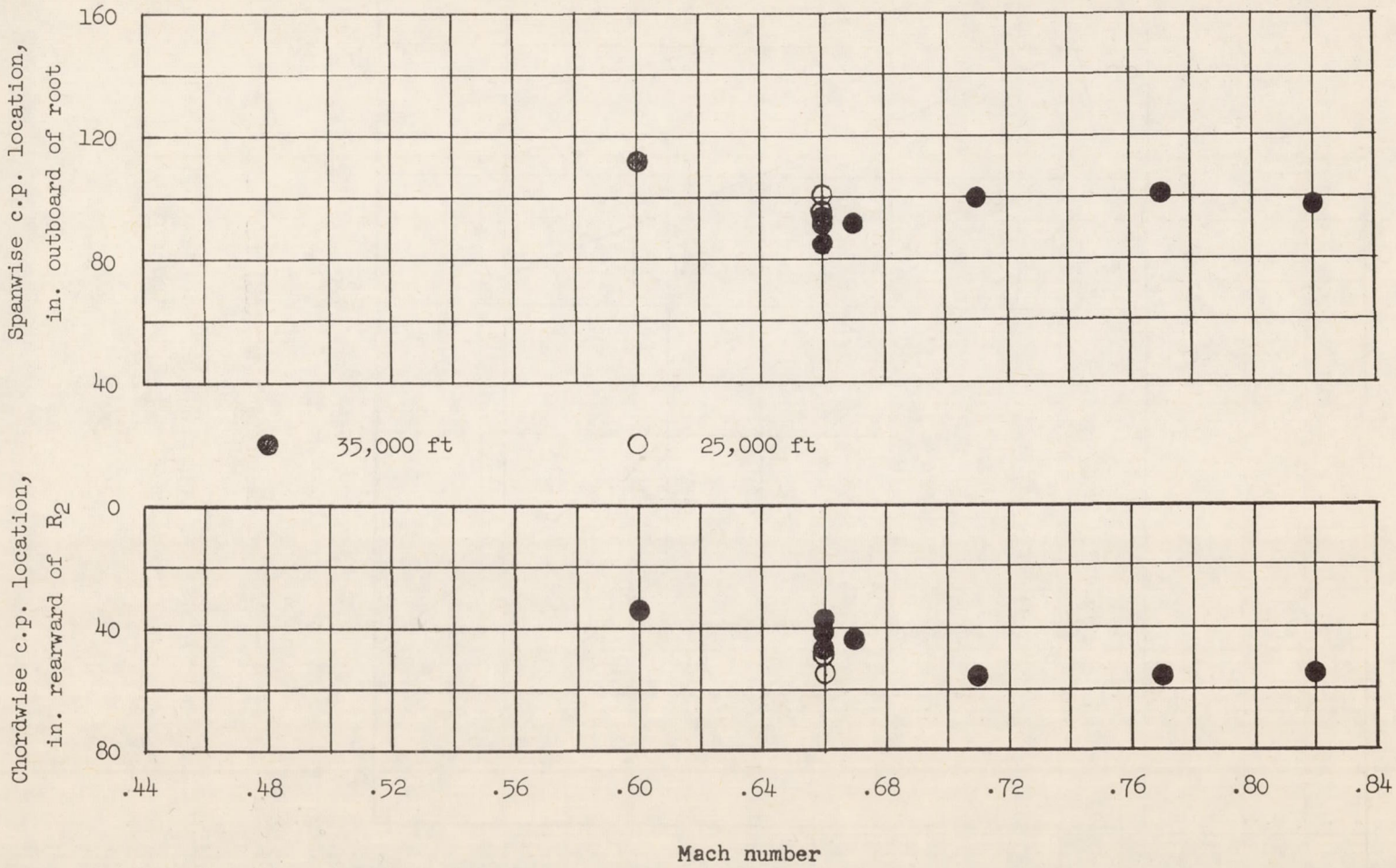


Figure 21.- Spanwise and chordwise center-of-pressure locations for the rudder-deflection vertical-tail load component for rudder-step maneuvers.

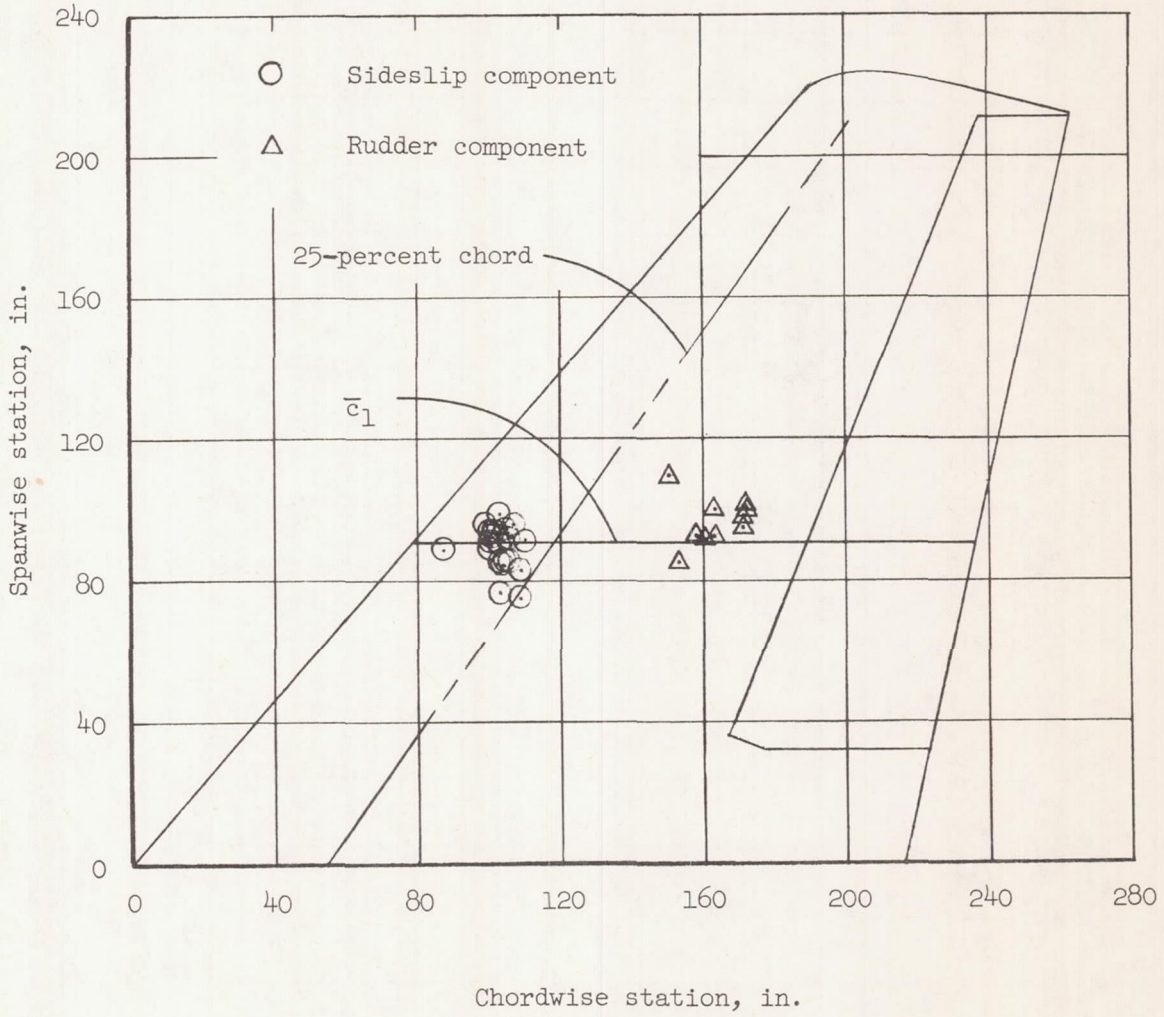


Figure 22.- Center-of-pressure locations of the vertical-tail sideslip and rudder-deflection load components.

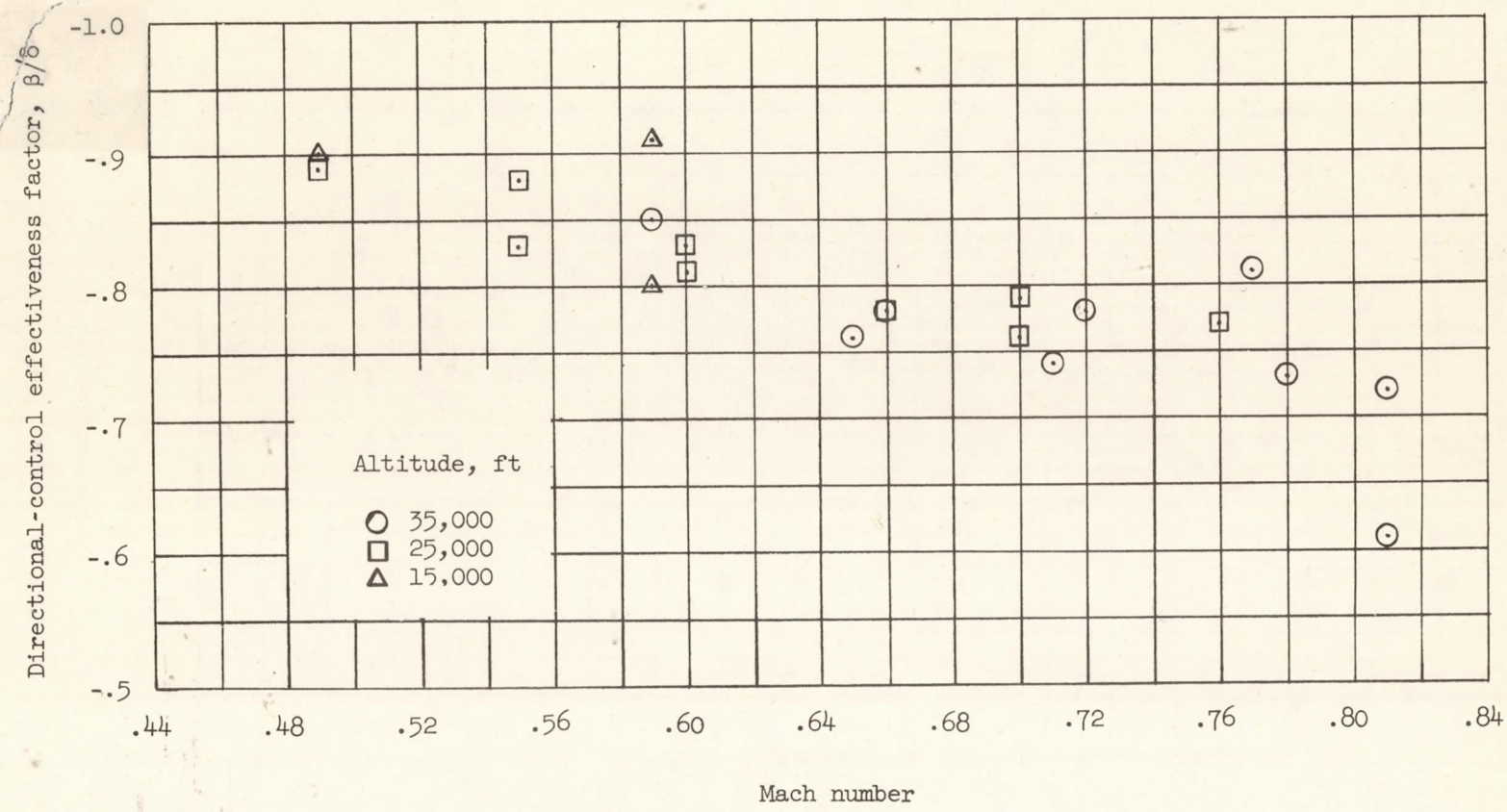


Figure 23.- Directional-control effectiveness factor β/δ as obtained from steady-sideslip maneuvers.

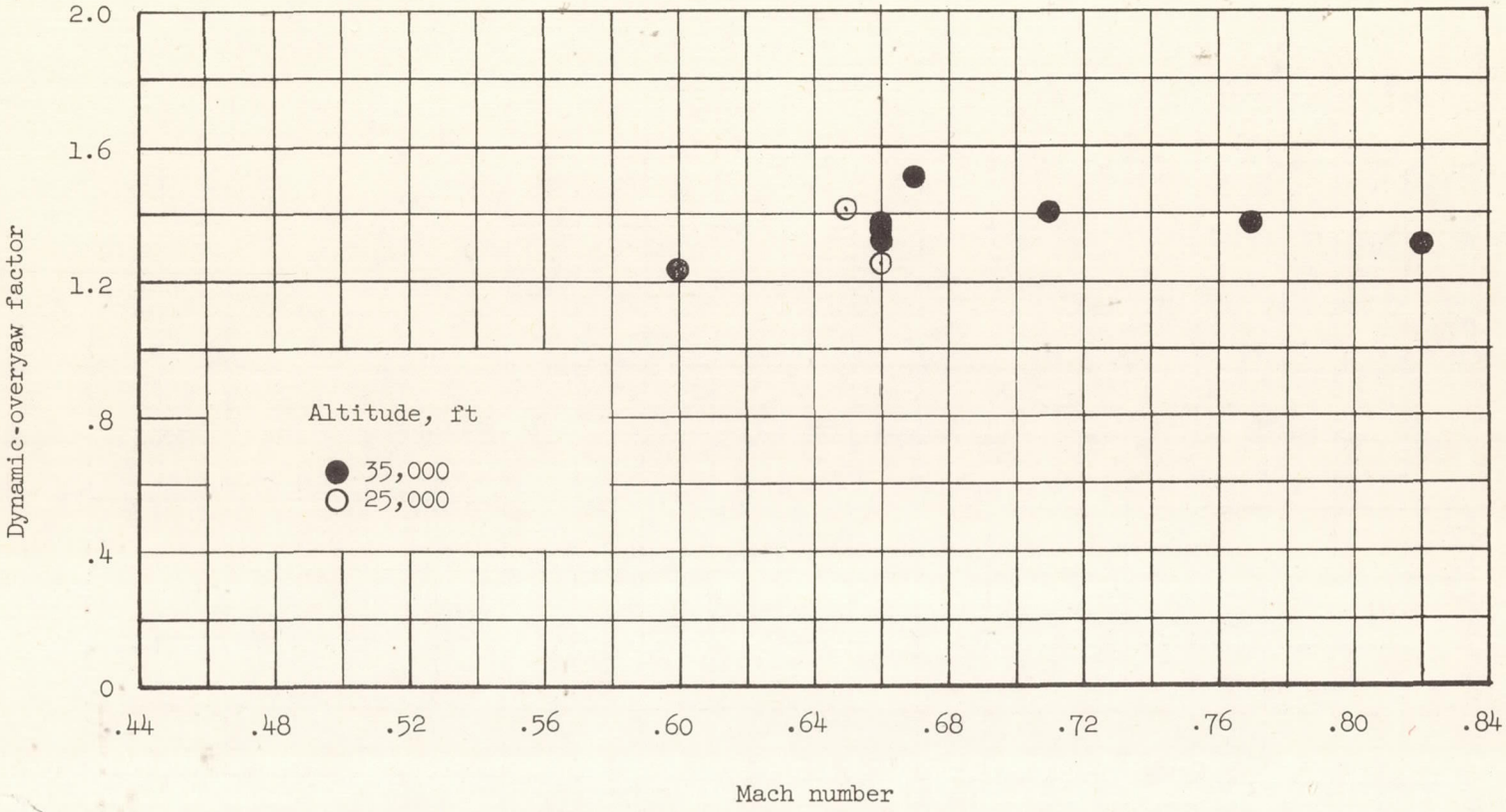


Figure 24.- Dynamic-overyaw factor.

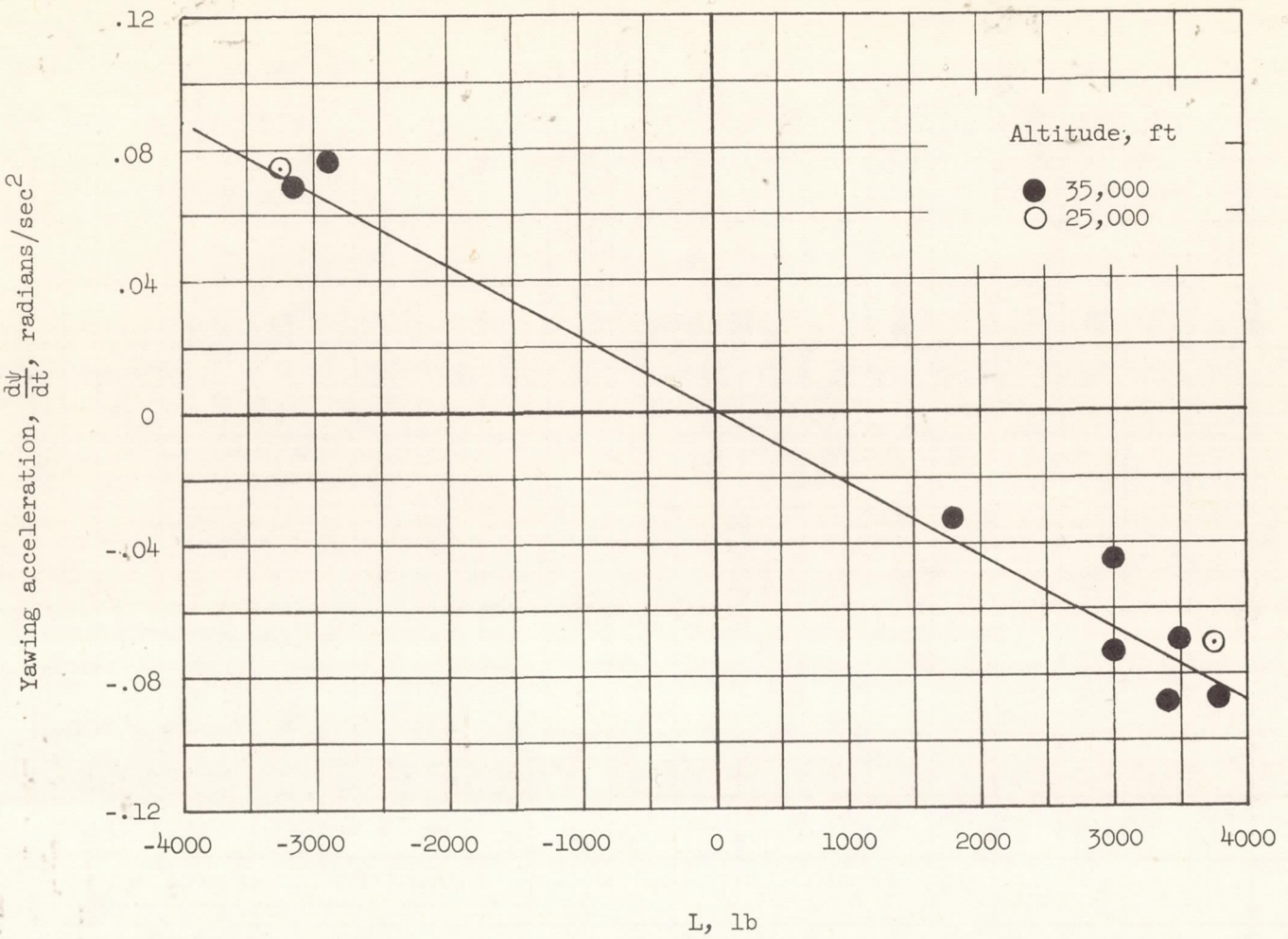


Figure 25.- The maximum yawing acceleration plotted against the maximum vertical-tail shear load as measured during several rudder-step maneuvers prior to the development of appreciable sideslip angle.

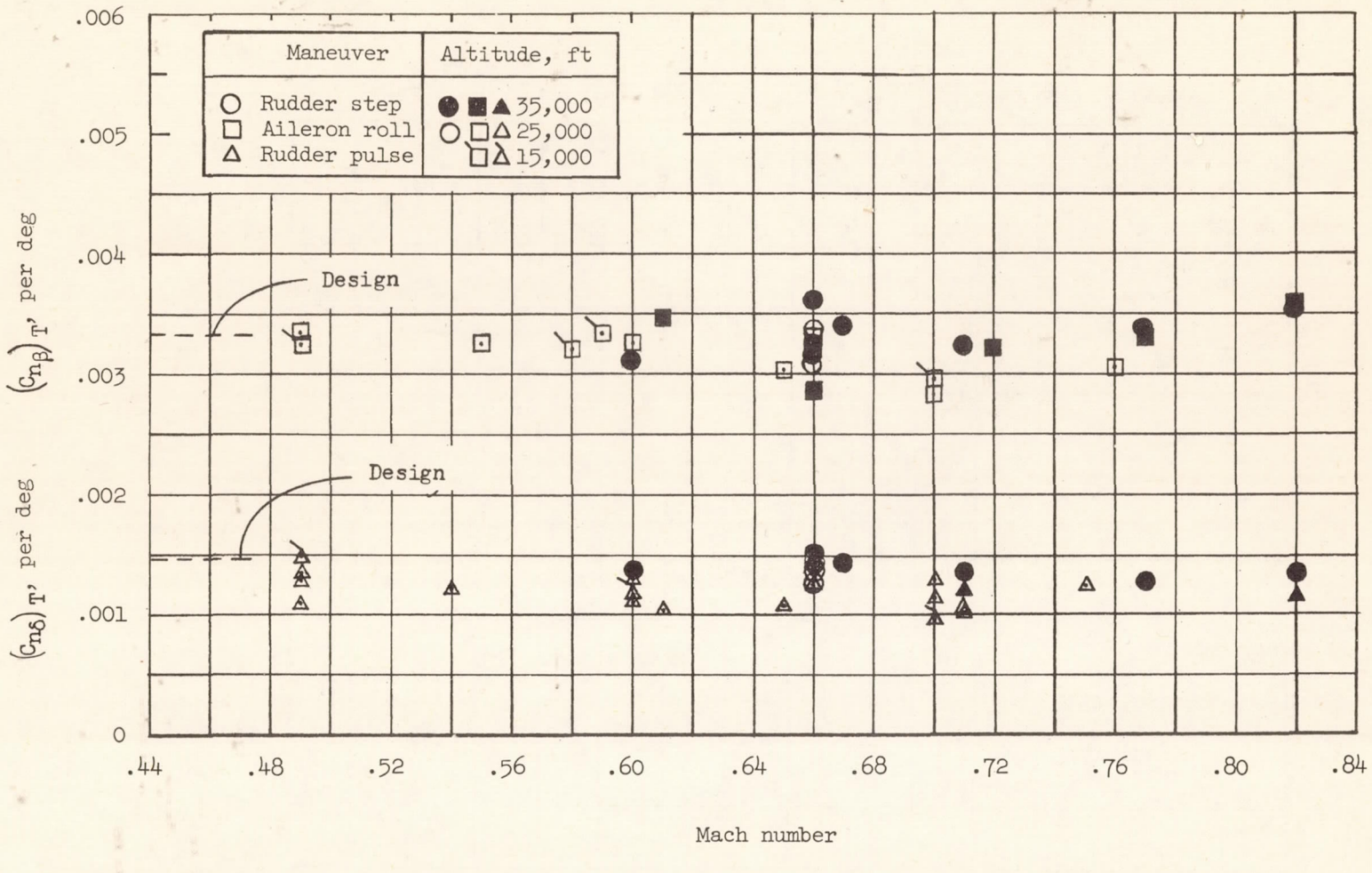


Figure 26.- Yawing-moment derivatives of the vertical tail and rudder.

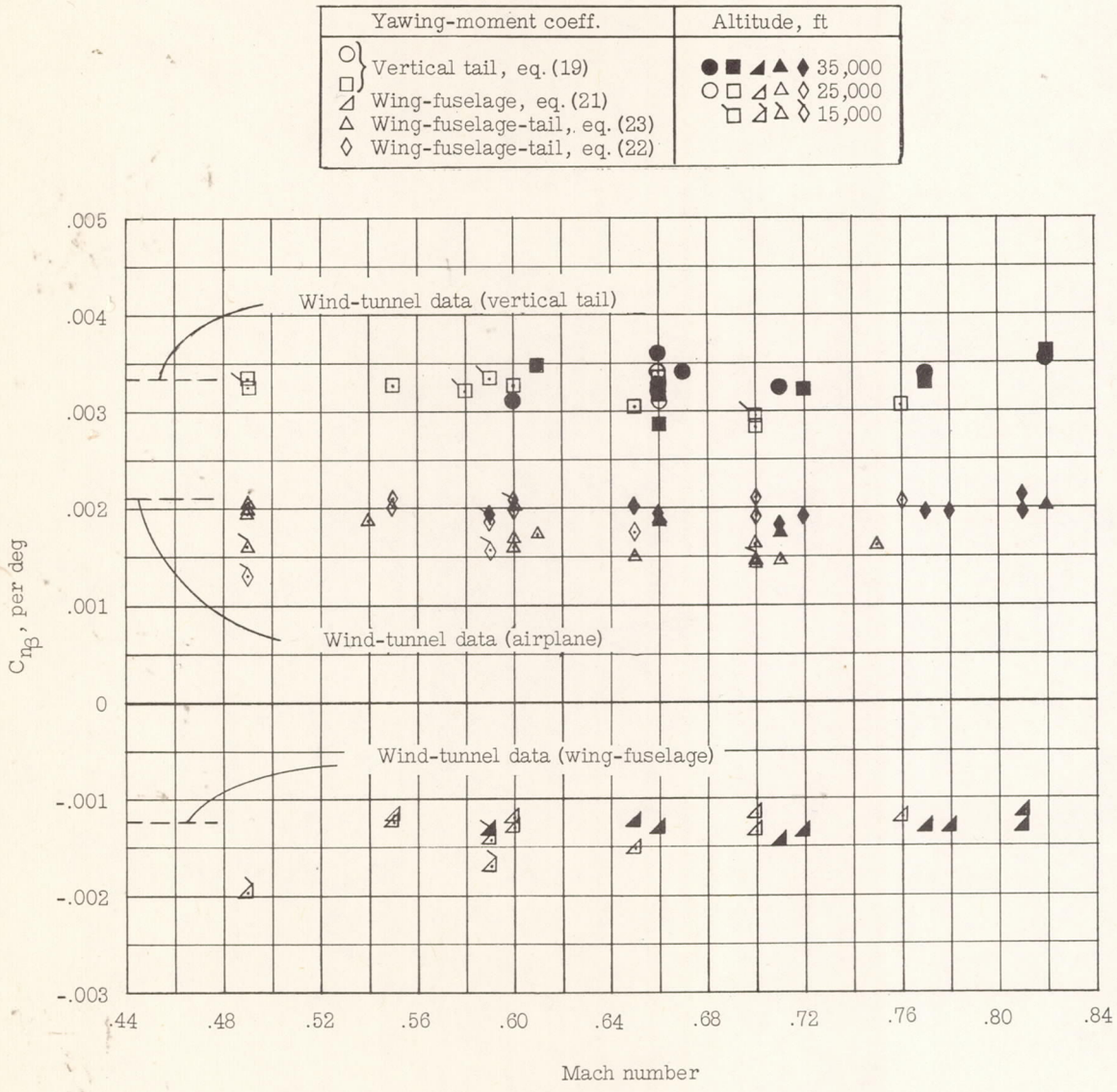


Figure 27.- Yawing-moment coefficients per degree of sideslip angle for the airplane, tail alone, and wing-fuselage combination.